Vertical Motion Structure in Maritime Continent Mesoscale Convective Systems: Results from a 50-MHz Profiler

ROBERT CIFELLI AND STEVEN A. RUTLEDGE

Department of Atmospheric Science, Colorado State University, Fort Collins, Colorado

(Manuscript received 17 May 1993, in final form 22 February 1994)

ABSTRACT

Wind profiler data were used to determine the vertical motion structure in four tropical mesoscale convective systems (MCSs), which occurred during the Down Under Doppler and Electricity Experiment (DUNDEE) near Darwin, Northern Territory, Australia. Three of the MCSs occurred during the monsoon-break convective regime and one occurred during the monsoon regime. In the break regime cases (each with a leading convective and trailing stratiform region structure), the wind profiler sampled low-level convective cells on the leading edge of the convective region, trailed by deeper updrafts of comparable magnitude. Surface rainfall measurements from a network of raingauges showed two comparable peaks in rainfall intensity that roughly corresponded to the passage of low-level and deep convective updraft (71%–80% of the system total rainfall was associated with the passage of the convective line). In the stratiform region, the profiler data showed generally weak vertical drafts (<1 m s^{-1}) and the presence of both mesoscale upward and downward motion (17%–28% of the system total rainfall was associated with the passage of the stratiform region). Deep subsidence in the transition zone located between the convective and stratiform regions was also documented in each of the break regime cases. Composite vertical motion profiles in different regions of the break MCSs were constructed and the salient features of the profiles are described. The composite vertical motion profiles are compared to similar profiles from different graphical regions.

The evolution of the monsoon MCS was different from the break regime cases. This system was characterized by a series of convective updrafts embedded in stratiform cloud.

1. Introduction

The global circulation is largely dependent on deep convection occurring in the Tropics. This deep convection often occurs in association with mesoscale convective systems (MCSs), which consist of not only deep convection, but regions of stratiform precipitation, with the latter being characterized by important mesoscale circulations. Both deep convection and mesoscale circulations act to couple the ocean, planetary boundary layer, and free troposphere through heat, moisture, and momentum transports. Riehl and Malkus (1958) focused on deep convection (hot towers) and identified their role in transporting heat from the planetary boundary layer to the upper troposphere. Since this early work, other studies have identified the important contributions of mesoscale vertical motions to heating and cooling the troposphere (Houze 1982; Johnson and Young 1983; Johnson 1984; Houze 1989; and others). Indeed, numerical model simulations have shown that the global circulation is sensitive to the vertical distribution of heating associated with tropical MCSs involving both convective and mesoscale processes (Hartmann et al. 1984; DeMaria 1985; Houze 1989; Hack and Schubert 1990; Johnson 1992). Since the vertical distribution of heating in an MCS is dominated by contributions involving phase changes of water (Houze 1989), which are in turn proportional to vertical motion profiles (convective and stratiform), it is important to continue to document these vertical motion profiles and to identify differences in the profiles with geographic location.

A number of studies have documented the vertical motion field within tropical MCSs [see Houze (1989) for a summary]. These studies have focused on vertical motion profiles of tropical MCSs from various parts of the equatorial region, including the eastern Atlantic Ocean region [GATE (GARP Atlantic Tropical Experiment)] continental west Africa [COPT 81 (Convection Profonde Tropicale)], the South China Sea [Winter MONEX (Monsoon Experiment), TAMEX (Taiwan Area Mesoscale Experiment)], the western Pacific (Pohnpei Island), and the oceanic regions off northern Australia [AMEX (Australian Monsoon Experiment), EMEX (Equatorial Mesoscale Experiment)]. These studies employed a variety of techniques to diagnose the vertical motion structure at a wide range of spatial scales, drawing on data from rawinsondes, Doppler radar, aircraft, and wind profilers.

Corresponding author address: Dr. Steven A. Rutledge, Dept. of Atmospheric Science, Colorado State University, Fort Collins, CO 80523.

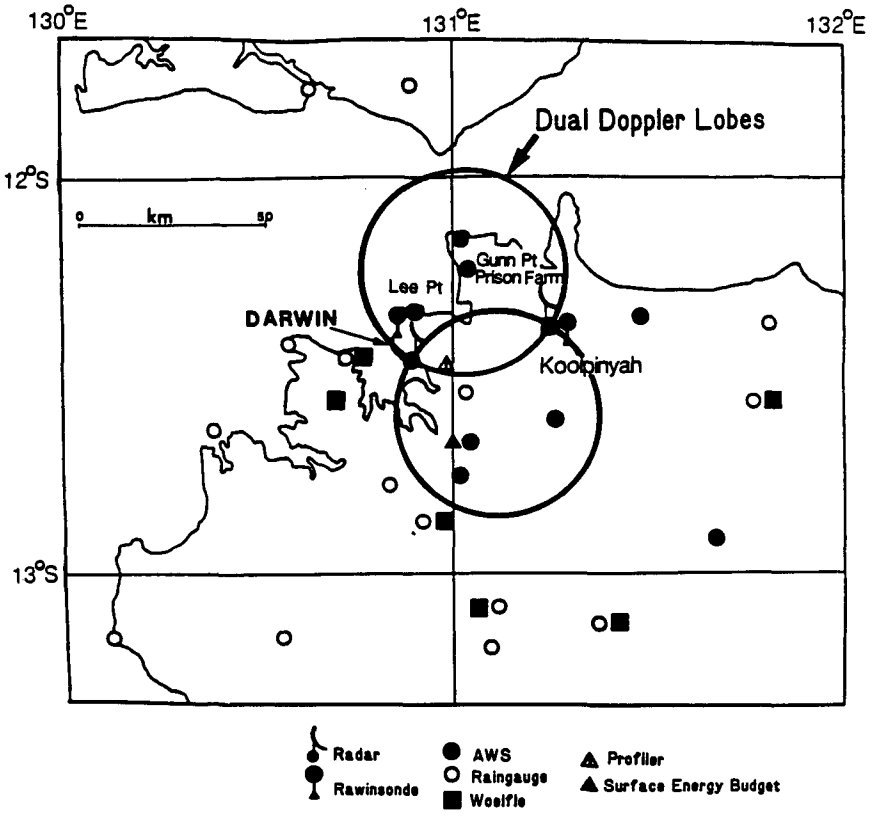

FIG. 1. Location of the observational network used during the DUNDEE field experiment [adapted from Rutledge et al. (1992)]. Note that only a portion of the Darwin area raingauge network is shown in this figure.

In this study, we describe the structure of vertical motion in four tropical MCSs using wind profiler data. The data were acquired during DUNDEE [Down Under Doppler and Electricity Experiment; Rutledge et al. (1992)] and therefore represent vertical motion in MCSs in the Maritime Continent region. Since we focus on continental tropical systems in this study (three out of four cases examined are continental in origin), our results complement the results from both AMEX and EMEX, which focused on oceanic systems. The high sampling rate of the wind profiler provided excellent resolution of vertical air motion within each MCS. Moreover, reflectivity data from 5-cm Doppler radars and surface rainfall data were used to correlate the vertical motion field with the vertical structure and precipitation features of the MCSs. The vertical velocity profiles were also composited to construct representative profiles of the vertical motion field in specific regions of the MCS. The resultant profiles are compared to vertical motion profiles from other tropical and middle latitude regions, in order to identify similarities and differences.

Determination of vertical motion profiles derived from MCSs in the northern Australia region [southern tip of the Maritime Continent, Ramage (1968)] is important for the following reasons:

1) these results are based on the direct observation of MCS vertical motion structure occurring in the Maritime Continent region and provide additional data from a largely undocumented region to compare with previously studied areas; and

2) the location of the DUNDEE field program (discussed below) provided a unique opportunity to study both tropical monsoon (oceanic) and monsoon-break (continental) convection and therefore to compare the vertical motion within these systems.

2. Methodology

Two 5-cm single Doppler radars [Massachusetts Institute of Technology (MIT) and Tropical Oceans Global Atmosphere (TOGA)] were used in conjunction with the 50-MHz NOAA/BMRC (National Oceanic and Atmospheric Administration/Bureau of Meteorology Research Centre) Darwin wind profiler to sample tropical convection during DUNDEE. The location of the radars and the wind profiler is shown in

TABLE 1. Characteristics of the MIT–TOGA radars and the Darwin wind profiler used during DUNDEE.

Characteristic	MIT	TOGA	Wind profiler
Wavelength (cm)	5.4	5.3	600
Peak power (kw)	250	250	30
Pulse length (μsec)	1.0	0.50, 1.9	6.7
Beamwidth (deg)	1.4	1.65	3.4
Minimum detectable signal (dBm)	−106	−113	−160
Pulse repetition frequency (s^{-1})	921	921	1000
Number of gates	226	224	50
Polarization	horizontal	horizontal	horizontal

Fig. 1. Characteristics of the MIT and TOGA radars, as well as the Darwin wind profiler, are shown in Table 1. Profiles of vertical motion were generated from the profiler data through a combination of a fully automated data processing technique based on a method described by Sato et al. (1990) and manual editing to analyze precipitation and clear-air turbulence components of the wind profiler spectral data.

The Darwin wind profiler operates at a frequency of 50 MHz, allowing both clear-air vertical motion and precipitation particle fall speeds to be measured directly (Carter et al. 1991). Moreover, during the DUNDEE field program, the profiler was operated with a single vertical incidence beam. Each profiler observation had a temporal resolution of 100 seconds. The unambiguous velocity was designed to automatically switch from ± 6 to ± 20 m s^{-1} whenever the Doppler spectral width exceeded the 6 m s^{-1} range (Carter et al. 1991). The unambiguous velocity of 20 m s^{-1} usually coincided with the occurrence of precipitation at the surface. In Fig. 2, we present examples of individual spectra collected with Nyquist velocities of ± 20 and ± 6 m s^{-1}. In Fig. 2a, the power returns at large negative radial velocity (toward the profiler) indicate hydrometeors falling toward the ground, while the power returns centered near zero radial velocity represent the clear-air turbulence component of the spectra. Note that the hydrometeor component can be identified to a height above 9 km in Fig. 2a. The "sawtooth" appearance of the spectra in the bottom gate of Fig. 2a was identified in many of the spectra used in

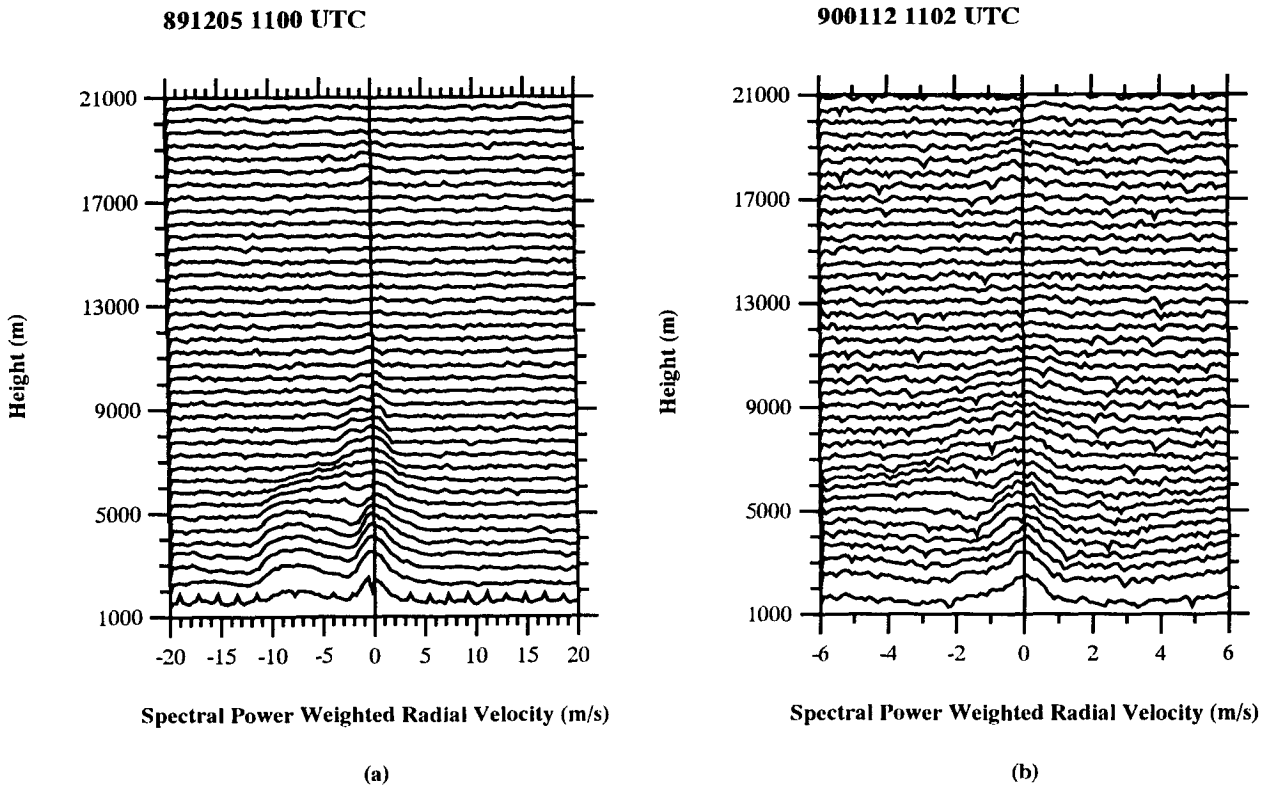

FIG. 2. Representative examples of individual profiler spectral data collected on (a) 5 December 1989 and (b) 12 January 1990. Positive (negative) radial velocities indicate upward (downward) motion in meters per second. Spectra observation times (UTC) are shown at the top of each plot. In (a) the spectra returns at large negative radial velocity represent the fall speeds of hydrometeors, while the spectra component centered near zero radial velocity is indicative of clear-air vertical velocity. Note the change in unambiguous velocity in (b) compared to (a).

this study. However, the anomaly, when present, was restricted to the first gate and did not appear to adversely affect the results of the curve-fit algorithm (described below). The "noisy" appearance of the ±6 m s^{-1} spectra compared to the ±20 m s^{-1} spectra in Fig. 2 is due to the greater radial velocity resolution at ±6 m s^{-1} (0.09 m s^{-1}) compared to ±20 m s^{-1} (0.31 m s^{-1}).

Prior to calculating the clear-air vertical velocity, the raw spectra were averaged in time to reduce random noise fluctuations and improve the statistical significance of the results. In the stratiform regions,[1] the individual spectra were averaged over an approximate 10-minute period (depending on the number of spectra used) in order to diagnose the mesoscale vertical motion pattern. Sensitivity analysis of the averaging period showed that the vertical velocity estimates in the stratiform region did not vary appreciably over intervals of 5–15 min (Fig. 3). In the convective portion of each MCS, the averaging time of the profiler data was reduced to approximately 4–5 min, due to large turbulence and spectral widths in the raw spectra. Longer averaging intervals in the convective region usually "smeared out" the precipitation and clear-air components of the spectra so that estimates of clear-air vertical velocity could not be accurately determined (see below). Because of the different averaging length intervals used in the convective and stratiform regions, the spatial scale sampled by the profiler in each region also varied, since this scale is dependent on the speed of the MCS relative to the profiler, the profiler beamwidth, and the length of the averaging interval. For the cases described herein, this spatial scale ranged from approximately 3–5 km during the passage of the convective line to 5–9 km in the stratiform regions.

Individual spectra were scrutinized to avoid contaminating the averaged results with spurious spectral power signals (i.e., radio interference, electrical discharges, etc.). As pointed out by Yoe et al. (1992), lightning can severely contaminate VHF wind profiler spectra. With the exception of one MCS (28 January 1990), the effects of lightning were rarely seen in the raw spectra.

For each of the MCSs we studied, the Nyquist interval occasionally alternated between ±6 and ±20 m s^{-1} during the passage of the stratiform region over the profiler. Because all of the average profiles were generated using only data with the same unambiguous velocity, the average profiles constructed in the stratiform region did not always contain the same number of raw spectra profiles, and the averaging time occasionally varied by a few minutes. Sensitivity analysis showed that, within a given averaging interval, the magnitude of clear-air vertical velocity in the stratiform region profiles was not particularly sensitive to the number of individual spectra used in the time averaging.

A number of different techniques have been utilized to separate the clear-air vertical motion from the hydrometeor fall speeds in VHF wind profiler spectral data. Some of the procedures include first-moment analysis of the Doppler spectra (Clark and Carter 1980), least squares fit of the Doppler spectra with one or two Gaussian approximations (Yoe et al. 1992), and least squares fit of the Doppler spectrum with a drop size distribution approximation for the hydrometeor component of the spectra and a Gaussian distribution for the turbulent component (Wakasugi et al. 1986; Wakasugi et al. 1987; Sato et al. 1990).

In this study, a combination of methods was developed to separate the clear-air signal from the precipitation signal in the averaged spectra. First, an algorithm to derive both atmospheric turbulence and precipitation parameters was developed based on the method described by Sato et al. (1990). The Sato et al. technique utilizes a Marshall–Palmer distribution to approximate the precipitation component of the spectra and a Gaussian distribution to fit the turbulence component to the observed Doppler spectrum $S(\nu)$ according to

$$S(\nu) = S_t(\nu) + S_p(\nu) * S_0(\nu) + P_n. \qquad (1)$$

In (1), $S_t(\nu)$ represents the Doppler power spectrum associated with backscatter from irregularities in the refractive index due to turbulence, ν is the frequency, P_n represents the noise level in the Doppler spectrum, and the asterisk denotes the convolution operation (Sato et al. 1990). Here $S_t(\nu)$ is approximated by the Gaussian function

$$S_t(\nu) = P_0 \exp\left[\frac{-(V-w)^2}{2\sigma^2}\right], \qquad (2)$$

where w is the mean radial wind velocity, σ is the spectral broadening, and V is the hydrometeor terminal fall speed. Here $S_p(\nu)$ represents the Doppler spectrum due to liquid precipitation and is approximated by

$$S_p(\nu) = C \cdot N(D) D^6 \left|\frac{d[V(D)]}{dD}\right|^{-1}. \qquad (3)$$

In (3), $N(D)dD$ is the number of raindrops per unit volume with diameters between D and $D + dD$, and C is a constant. The explicit relation between D and V is provided in Sato et al. (1990).

The term $S_0(\nu)$ in (1) is a normalized form of $S_t(\nu)$ and is given by

$$S_0(\nu) = \frac{1}{(2\pi)^{1/2}\sigma} \exp\left[\frac{-(V-w)^2}{2\sigma^2}\right]. \qquad (4)$$

The convolution operation implies that the raindrops instantaneously respond to atmospheric turbulence

[1] The partitioning of each MCS into convective, transition, and stratiform regions is described in section 4b.

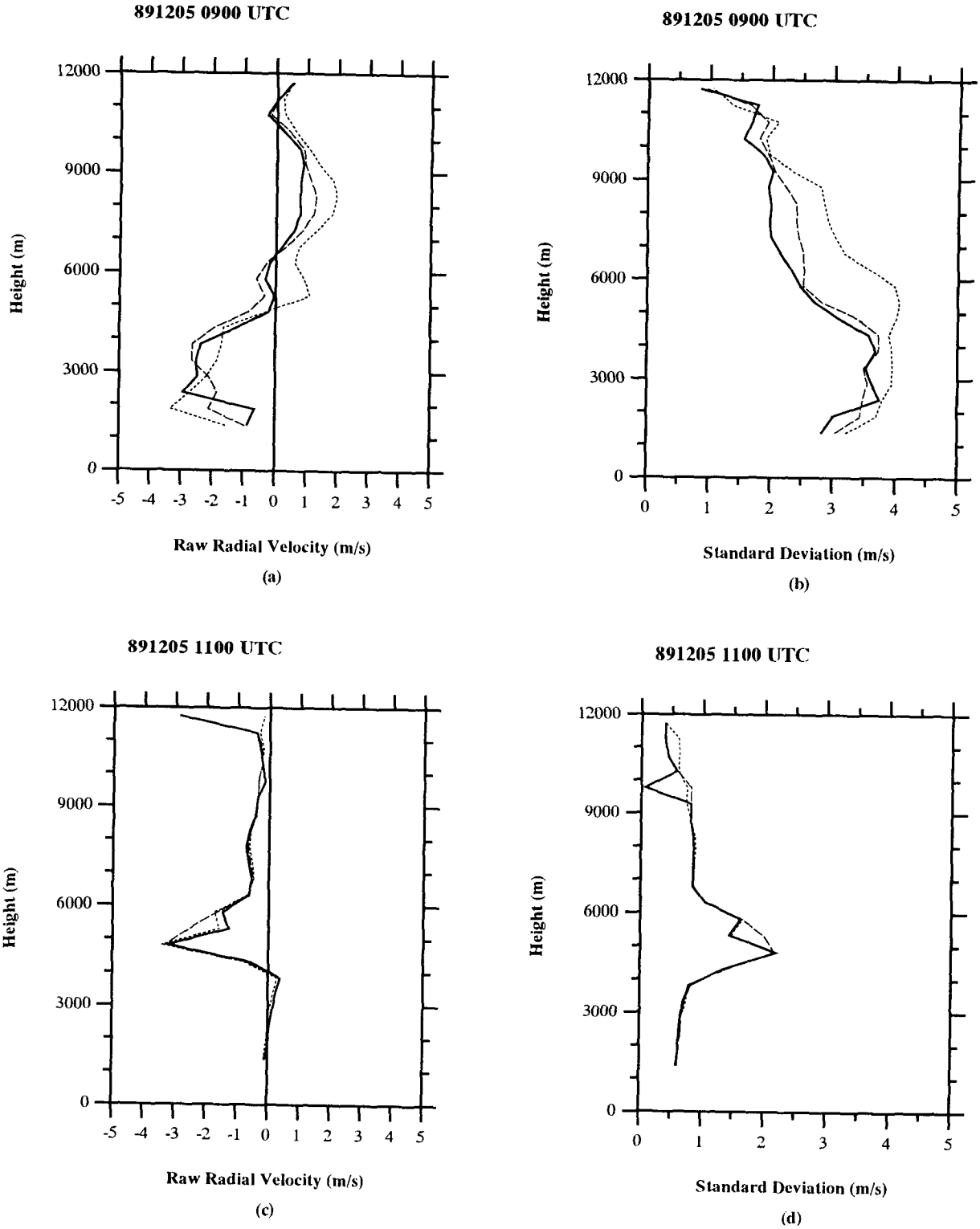

FIG. 3. Representative profiles of mean clear-air vertical motion and standard deviation for the 5 December 1989 MCS using the results of the curve-fit algorithm. In (a) and (b), spectra were collected during the passage of the convective line (0900 UTC), while profiles in (c) and (d) represent spectra collected under stratiform conditions (1100 UTC). The solid, long-dashed, and short-dashed lines represent the profiles obtained after averaging the spectra over 5, 10, and 15 minutes, respectively, and running the curve-fit algorithm. In (a) and (c), positive (negative) vertical velocity indicates upward (downward) motion. Note the relatively large changes in radial velocity and standard deviation between the different profiles in the convective region compared to similar profiles in the stratiform region. Also note that the radial velocities have not been adjusted to account for particle fall speed biases (see text for details).

(Wakasugi et al. 1987). In practice, a window function is usually applied to the Doppler spectrum $S(\nu)$ to account for data truncation effects and to improve the curve fit along the edges of the Doppler spectrum (Wakasugi et al. 1986). Because the analysis objective was only to determine the mean vertical velocity, no windowing function was used in this study.

Sensitivity analysis with the curve-fit program showed that the algorithm provided reasonable "fits" to the profiler spectra below the melting level and above about 9 km (AGL); however, in the region between 4.5 and 9 km, the curve-fitting algorithm was often unable to distinguish between the clear-air and precipitation signal peaks (Fig. 4). This was probably due to the existence of water drops, snow, and other ice hydrometeors in the mixed phase region of the cloud (Carter et al. 1991). Because the mixed phase hydrometeor species have different fall speeds, the Doppler spectra from the turbulence and precipitation components "merged together" and the curve-fitting algorithm attempted to fit both the turbulence and precipitation spectra with a single Gaussian curve (Fig. 4b). In other words, the algorithm was unable to separate clear-air vertical motion from the hydrometeor motion. Merging of the precipitation and turbulence Doppler spectra caused the center of the Gaussian curve fit (i.e., mean vertical velocity) to be shifted to the left (i.e., toward negative radial velocities) relative to the center of the turbulence peak power spectra. Similar difficulties in separating the clear-air vertical velocity from particle fall speeds using a VHF profiler were reported by Chilson et al. (1993) during sampling of a thunderstorm over Puerto Rico; however, in that case, data from a collocated UHF profiler were utilized to help extract the clear-air component.

In situations where merged Doppler spectra occurred, a second analysis technique was required to extract the clear-air signal from the precipitation signal. In these cases, the center of the Gaussian was manually edited so that the mean clear-air vertical motion coincided with the approximate location of the turbulence peak power. Although the location of the mean clear-air position was usually obvious by visual inspection (Fig. 4), the error associated with this procedure was difficult to quantify (see below), and the possibility of particle fall speed bias in the clear-air estimates cannot be entirely ruled out. In general, the precipitation spectra component decreased significantly above about 9 km so that the program was able to fit the total Doppler spectra reasonably well with a single Gaussian approximation.

For each of the four MCSs we studied, approximately 3.5–4.5 hours of wind profiler data were obtained as the systems passed over the profiler site. A total of 97 averaged spectral profiles were constructed for all four of the MCSs (approximately 24 for each system). This allowed for the construction of time–height cross sections of vertical velocity with high temporal resolution (10 minutes) during the passage of each system; however, we will restrict our discussion of time–height cross sections to two MCSs, the monsoon case and one of the monsoon break cases.

In Fig. 5, we show composite profiles of several statistical parameters associated with the curve-fit algorithm to quantify potential errors in the clear-air vertical velocity estimates. These statistics were generated in each storm region (e.g., convective, transition, and stratiform) using all of the averaged spectra from the three break monsoon cases (similar statistics were not generated for the monsoon regime since only one system was analyzed).

Figure 5a shows the mean composite clear-air standard deviation profile of the averaged spectra for the convective, transition, and stratiform regions as determined by the curve-fit procedure. Since this statistic was generated by the curve-fit algorithm, it provides a

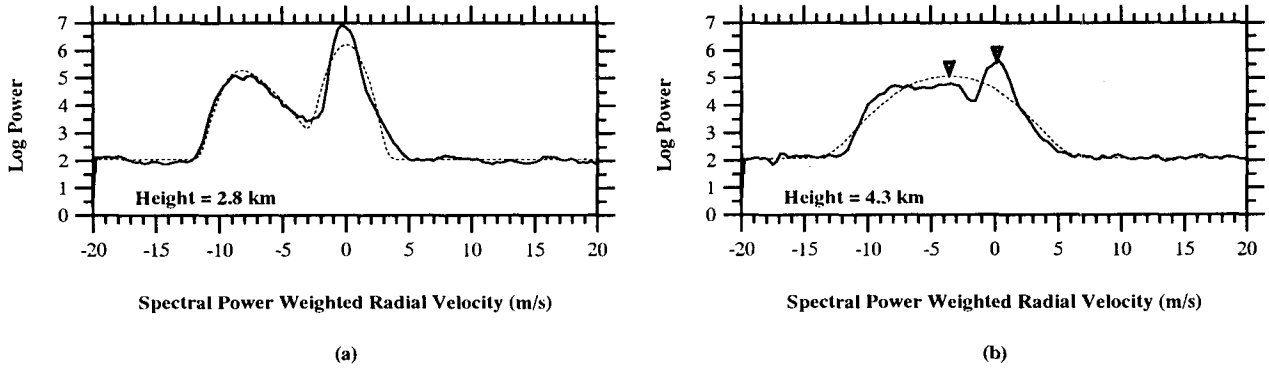

FIG. 4. Ten-minute averaged spectra collected at 1100 UTC 5 December 1989 at (a) 2.8 km and (b) 4.3 km. The solid line shows the observed spectra data with the left peak indicating hydrometeor fall speed and the right peak indicating clear-air vertical velocity. Positive (negative) radial velocities represent upward (downward) motion. The dashed line represents the results of the curve-fit algorithm. In (b) the left (right) triangle indicates the clear-air vertical velocity estimate selected by the curve-fit algorithm (manual editing). Note the change in shape of the precipitation component of the spectra in (b) compared to (a).

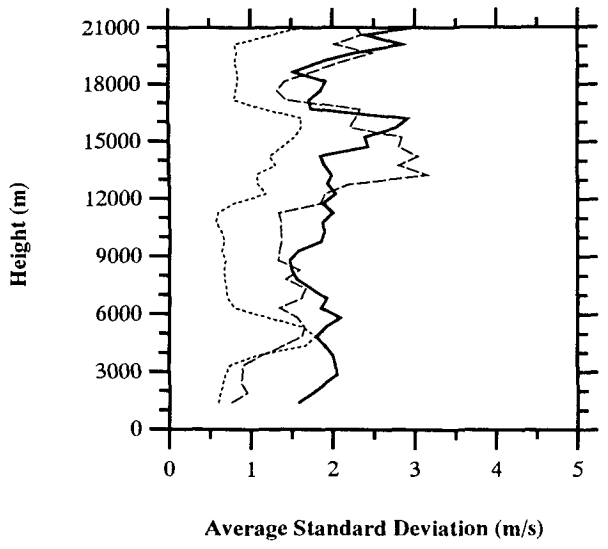

(a)

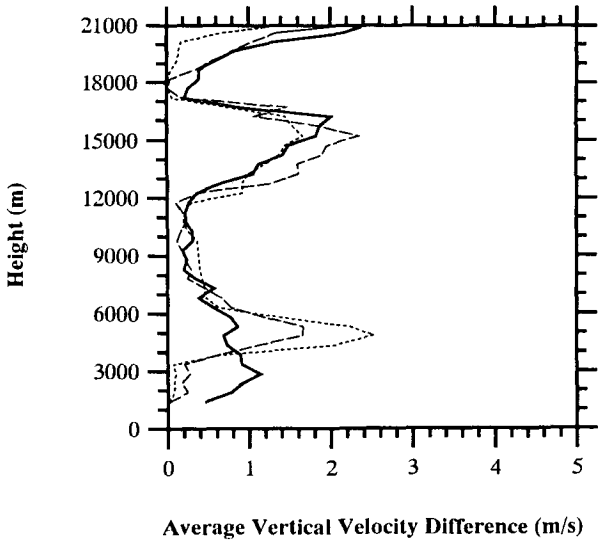

(b)

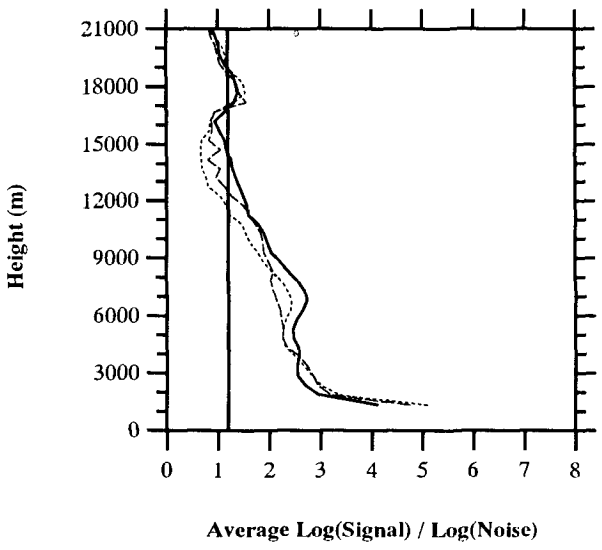

(c)

FIG. 5. Composite profiles for the convective (solid line), transition (long-dashed line), and stratiform (short-dashed line) regions of the three monsoon-break MCSs, based on results from the curve-fit algorithm. (a) Standard deviation. (b) Vertical velocity difference calculated as the absolute value difference of the clear-air vertical velocity estimate generated by the curve-fit algorithm and the manually edited value. This statistic indirectly measures the degree of spectra merging in the data (see text for details). (c) Signal-to-noise ratio, log(signal power)/log(noise power).

measure of clear-air vertical velocity variance in regions where the algorithm generated reasonable fits to the spectra (i.e., no merging of the turbulence and precipitation components). The degree of spectra merging is indicated in Fig. 5b, which shows profiles of the average difference (absolute value) of the curve-fit and manually edited clear-air vertical velocity estimates (hereafter referred to as velocity difference) for each storm region. This parameter indicates the magnitude of the bias in the program-derived clear-air vertical velocity estimate due to particle fall speed contamination. In regions where the algorithm identified separate spectra components for precipitation and turbulence, the magnitude of the velocity difference is relatively small, indicating that the corresponding standard deviation values are reasonable estimates of the dispersion of clear-air vertical velocity around the mean value. However, in places where the clear-air and precipitation spectra components merged, the difference in vertical velocity estimates is large due to the particle fall speed bias (compare Figs. 4a and 4b). In these situations, the program usually generated a single curve fit and assigned a standard deviation value based on the combined width of the clear-air and precipitation components. Therefore, the standard deviation values in the region of merged spectra shown in Fig. 5a pro-

vide conservative estimates of the variability of clear-air vertical velocity. More accurate estimates of the clear-air standard deviation alone would require a very subjective estimate of the shape of the turbulence spectra component and resulting Gaussian curve-fit inflection point.

In the convective region, the profile of composite standard deviation is relatively large (1.5–2.0 m s^{-1}) with a peak in the lower troposphere, reflecting the existence of broad spectra (Fig. 5a). The large standard deviations in the lower troposphere are coincident with large magnitudes of the velocity difference profile (Fig. 5b), indicating that the convective region standard deviations are most affected by spectra merging in the lower troposphere. In the stratiform region, the shape of the standard deviation profile is significantly different from the convective region. The magnitudes of the composite stratiform standard deviation profile are on the order of 0.65–0.7 m s^{-1} below about 3.5 km and above 6.5 km, significantly less than the corresponding composite convective region profile (Fig. 5a). In the vicinity of the melting level (approximately 5 km), the standard deviations in the stratiform region are of similar magnitude to the convective region (>1 m s^{-1}) due to the large hydrometeor component of the spectra relative to the clear-air and the resulting spectra merging (Fig. 5b). Clear-air velocities were shifted over 2 m s^{-1} on average (to more positive values) to correct for particle fall speed contamination in this region. Moreover, as can be seen from Fig. 5b, the magnitude of the particle fall speed bias gradually tapers off with height above 6.5 km (similar to the convective region profile), as the strength of the hydrometeor spectra component is reduced. As expected, the magnitude and shape of the composite transition zone profile has similar characteristics to both the convective and stratiform regions.

An arbitrary threshold of signal to noise was developed to determine whether the signal at a particular level represented meteorologically significant data or was part of the noise spectrum. If the ratio of log(signal power)/log(noise power) determined by the curve-fitting algorithm was below 1.2, it was assumed that the signal was not significant and a vertical velocity value was not obtained for that level. Since the signal power decreased gradually with height, there were many borderline cases where the ratio was approximately 1.2. In these situations, continuity of the velocity and width of the turbulence Doppler spectra with spectra at lower levels (where the threshold was exceeded) was used to determine whether the signal at the level in question was meteorologically significant. Figure 5c shows composite profiles of log(signal power)/log(noise power) for the convective, transition, and stratiform regions of all three break monsoon cases. Also shown in Fig. 5c is the threshold value of 1.2. On average, the clear-air spectra were deemed significant up to about 11 km in the stratiform region and to about 14 km in the convective region. In the region between about 14 and 17 km, the composite signal-to-noise profiles were below the threshold of 1.2 and were not treated as representing meteorologically significant data. The magnitude of standard deviation and the velocity difference profiles (Figs. 5a and 5b) are relatively large in this same height region due to the low signal-to-noise ratio and resulting poor curve fits. Note, however, that the ratio of signal to noise increased above the threshold in the vicinity of the tropopause (17–19 km) for all three composite profiles, indicating the return of the clear-air signal to meteorologically significant levels in this region.

Additional errors in deriving vertical velocity measurements from 50-MHz wind profiler data can occur due to aspect sensitivity (Larsen et al. 1991). This error occurs when the refractive layers (providing turbulence backscatter) are inclined with respect to the horizontal plane. Because the strongest scatter is produced in a direction perpendicular to the refractive layer, tilted layers will allow a component of the horizontal wind to be resolved along with the projection of the vertical component along the effective beam direction (Larsen et al. 1991). Since the Darwin profiler was only operating in a vertically pointing mode during the 1989/90 DUNDEE season, it is impossible to quantify the potential error induced by aspect sensitivity.

Data from Geostationary Meteorological Satellite (GMS) images were available at approximately 3-hour intervals for each of the MCSs we studied. These images were used to compare the location of the cloud top (based on brightness temperature) with the radar-inferred echo top and the upper boundary of vertical motion sampled by the wind profiler. Because of the relatively short duration of each MCS and the approximate 3-hour interval between satellite images, there were usually only one or two overlapping times where all three remote sensing instruments (radar, wind profiler, satellite) were collecting data simultaneously. An average value of cloud-top temperature was determined for each image over the location of the observational network. Sounding data (usually 1200 UTC from Darwin) were used to construct plots of cloud-top temperature versus geopotential height and to assign an average cloud-top height over the observational network. Caution should be applied to cloud-top heights based on IR satellite data since factors such as range resolution can produce ambiguous estimates of cloud-top heights (Adler and Markus 1982). In this study, we use the GMS data only for comparison purposes.

Data from both the MIT and TOGA radars were used to construct time–height cross sections of radar reflectivity over the profiler. Radar volumes were analyzed approximately every 10 minutes to achieve temporal resolution similar to the wind-profiler data. In cases where radar data were unavailable, linear interpolation was used to "fill in the gaps" of the reflectivity cross sections. Whenever possible, these reflectivity cross

sections were generated with MIT data since the location of this radar relative to the wind profiler allowed for reflectivity data to be examined over the profiler up to a vertical distance of about 12 km. In cases where MIT data were unavailable (e.g., the onset of convection of the 12 January 1990), TOGA data were used to construct the time–height reflectivity cross sections. Because of the close proximity of the TOGA site to the profiler, the actual location of the cross section using TOGA data was approximately 20 km east of the profiler along the baseline toward the MIT radar site.

Surface rainfall data were available from the Darwin area raingauge network (Fig. 1). This network covers an area exceeding 45 000 km^2 centered on the TOGA radar. Most of the gauges are located within 75 km of Darwin to correlate radar and raingauge rainfall estimation for Tropical Rainfall Measuring Mission (TRMM) objectives (Simpson et al. 1988). Rainfall was recorded digitally using a tipping-bucket gauge. The tipping bucket recorded data whenever rainfall accumulation exceeded 0.2 mm (T. Keenan 1993, personal communication). Data from the Berrimah raingauge (TOGA radar site) were used to compare rainfall with vertical velocity measured with the wind profiler. This particular raingauge was the closest raingauge to the wind profiler in the network. Due to system malfunction, data from the Berrimah site were not available during the passage of one of the MCSs we studied (12 January 1990). In this case, we used data from the Koolpinyah raingauge site (coincident with the MIT radar location). Due to the large spatial variability of rainfall amounts within each of the break regime MCSs (described below), data from the Darwin area raingauge network were used to compute rainfall statistics in these systems. A discussion of the rainfall statistics analysis is presented in section 4c.

3. Convective regimes in northern Australia

Darwin is located at the southern tip of the Maritime Continent and experiences a monsoon-type climate (Holland 1986). The onset of the active (wet) period usually occurs in December and typically lasts through late February. During the wet season, there are two convective regimes that occur over tropical northern Australia: monsoon and break (Rutledge et al. 1992). Monsoon convection occurs when the axis of the ITCZ moves south of the Darwin area, providing deep west-northwesterly flow from over the ocean and placing the continental northern Australia region in a maritime air mass. Break period convection occurs when the axis of the ITCZ is north of Darwin. This juxtaposition of the monsoon trough results in low-level southeasterly flow over the "top end" of northern Australia and allows strong surface heating and intense continental convection to develop. On average, break period conditions occur during approximately 20% of the summer monsoon season with a mean period of 40 days (Holland 1986).

As pointed out by Keenan and Carbone (1992), the primary trigger for both monsoon and break regime MCSs is driven by land and sea-breeze circulations. Keenan and Carbone (1992) have noted that both monsoon and break MCSs tend to initially align parallel to the lower-tropospheric shear but later evolve to an orientation perpendicular to the low-level shear. The four MCSs used in the analysis include three break regime cases (5 December 1989, 22 January 1990, 28 January 1990) and one monsoon regime case (12 January 1990).

4. Results

a. *Case descriptions and time–height sections of vertical motion*

In this section, we describe the vertical velocity structure of one break monsoon MCS as well as the monsoon MCS in detail. Composite results using data from a total of three break monsoon MCSs will be presented in section 4b.

1) 5 DECEMBER 1989

The 0000 UTC 5 December 1989 Darwin sounding is shown in Fig. 6. The moisture profile shows a relatively dry surface layer with nearly saturated conditions at 875 and 550 mb. The lapse rate exceeds moist adiabatic from the surface up to about 550 mb. This layer is also characterized by southeasterly flow that extends from the surface up to 500 mb. Above this level, the

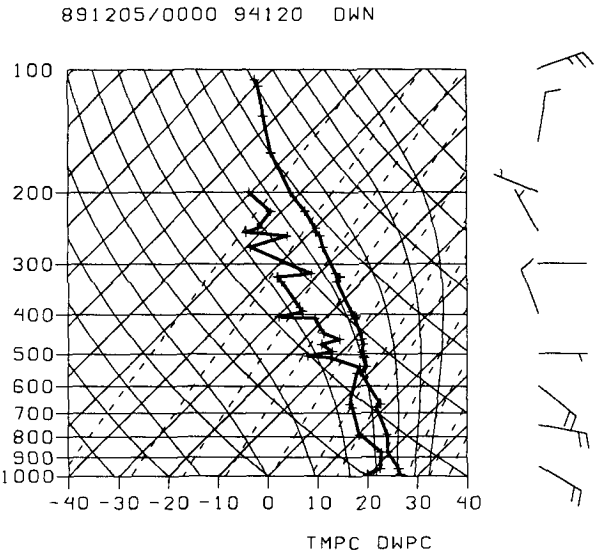

FIG. 6. Skew-T plot of upper-air sounding from Darwin at 0000 UTC 5 December 1989. Temperature and dewpoint traces (°C) are indicated by the bold solid lines. Wind data are shown in the right portion of the figure with wind speed (knots) represented by the length of the barb (long barb: 10 kt; short barb: 5 kt).

flow reverses and contains a significant northerly component.

The 5 December 1989 MCS (hereafter referred to as 5Dec89) formed approximately 80 km south of the Darwin area during monsoon-break conditions. Initially, the MCS consisted of scattered convective cells, but later consolidated into a solid line oriented east–west (Rasmussen and Rutledge 1993). The system moved to the north at approximately 8–10 m s^{-1}, passing over Darwin, and then out to sea. The maximum vertical extent of radar echoes in the convective line was approximately 18 km. The line weakened as it approached Darwin, coincident with the development of a trailing stratiform region. The convective region passed over the observational network between 0850 and 0930 UTC. The stratiform region was sampled with both the surface radar and wind profiler up until 1200 UTC.

Time–height cross sections of radar reflectivity, vertical air velocity, and surface rainfall for this case are shown in Fig. 7. The cross sections encompass approximately 3.5 hours of the passage of this system. Low-level reflectivity plots for this case (at selected times) are shown in Fig. 8. Contrasting the low-level reflectivity pattern (Fig. 8) with the cross sections of reflectivity, surface rainfall, and vertical velocity (Fig. 7), it can be seen that the squall line's leading edge passed over the profiler near 0840 UTC. At this time, an updraft with magnitudes up to 4.5 m s^{-1} was situated in the lower troposphere, at the leading edge of the MCS. Above about 7 km, a weaker ascent region extended through the troposphere. Relatively weak downdrafts (<1 m s^{-1}) were situated between the lower- and upper-troposphere ascent regions. Vertical cross sections generated with MIT radar data (not shown) suggest that this leading region of low-level ascent was associated with the development of new convection along the leading edge of the MCS. This leading low-level updraft developed as the system tilted rearward (i.e., the opposite direction toward which the line was moving) and persisted for several hours after the convective region passed over the observational network. The characteristic tilting of convective cells along the leading edge of MCSs has been previously documented in both middle latitude and tropical MCSs (Houze 1977; LeMone et al. 1984; Smull and Houze 1987; Rasmussen and Rutledge 1993). The reflectivity cross section (Fig. 7a) indicates a rapid decrease in reflectivity above the melting level (near 0900 UTC) associated with the low-level updrafts. Szoke et al. (1986) and Jorgensen and LeMone (1989) documented sharp decreases in reflectivity above the melting level in tropical convection and suggested the reflectivity gradient was due to the inability of the updraft to carry large drops a significant distance above the 0°C level. The profile in Fig. 7a suggests low-level precipitation generation by collision–coalescence processes. Inspection of the rainfall intensity trace (Fig. 7c) shows that a sharp peak in rainfall intensity (72 mm h^{-1}) occurred near 0900 UTC, in association with the low-level updraft peak.

Between 0910 and 0920 UTC, a deep updraft core with magnitudes exceeding 9 m s^{-1} passed over the profiler site (Fig. 7b), with maximum ascent centered between 9 and 10 km. Based on extrapolation of data compiled by Jorgensen and LeMone (1989; their Fig. 4) the magnitude of this updraft is greater than the strongest 10% average updraft reported for tropical oceanic systems, but is less than the value reported for continental systems studied in the Thunderstorm Project (i.e., the regions of central Florida and Ohio).

This deep updraft was flanked by subsidence (1–2 m s^{-1}) at upper levels. The position of the downdrafts is remarkably similar to downdrafts in other squall line studies diagnosed from dual-Doppler analyses (Heymsfield and Schotz 1985; Smull and Houze 1987; Biggerstaff and Houze 1993). Coincident with the strengthening of the maximum ascent region in the middle troposphere, the reflectivity cross section shows a sharp increase in reflectivity above the melting level with the 20–30-dBZ contour extending up to about 10 km (Fig. 7a). The relatively large reflectivities (up to 30 dBZ) collocated with the strong upward motion are likely associated with the presence of graupel and supercooled water. The shift of the maximum updraft to the middle troposphere and the increase in reflectivity above the 0°C level reflect the passage of mature, deep convective cells across the profiler site at this time. A secondary peak in rainfall intensity occurred at 0910 UTC in conjunction with the passage of the deep updraft core in the middle troposphere. To the extent that the single raingauge trace (Fig. 7c) represented the rainfall rates associated with the passage of the leading edge of the MCS, it is important to note that the peak rainfall rates associated with the low-level updraft and the deeper middle to upper troposphere updraft are similar in magnitude (72 and 62 mm h^{-1}, respectively). A similar bimodal structure was evident in most of the DUNDEE raingauge traces for all three of the break regime MCSs (section 4c). The low-level reflectivity plots (Fig. 8b) indicate the development of a stratiform region south of the observational network during this time period.

Deep subsidence occurred over the profiler throughout most of the troposphere from 0940 to 1010 UTC (Fig. 7b). The magnitude of this subsidence was on the order of 1.5 m s^{-1}. The deep subsidence feature coincided with a reflectivity trough (transition zone) in both the reflectivity cross section (Fig. 7a) and the low-level reflectivity pattern (Fig. 8c). The reflectivity trough was most pronounced in the upper and lower troposphere and was separated by a region of higher reflectivity at middle levels (4–6.5 km). Although the precise relationship between the upper and lower reflectivity minimum is not clear, the trough below the melting level could be related to melting and evaporation of hydrometeors in the presence of a downdraft.

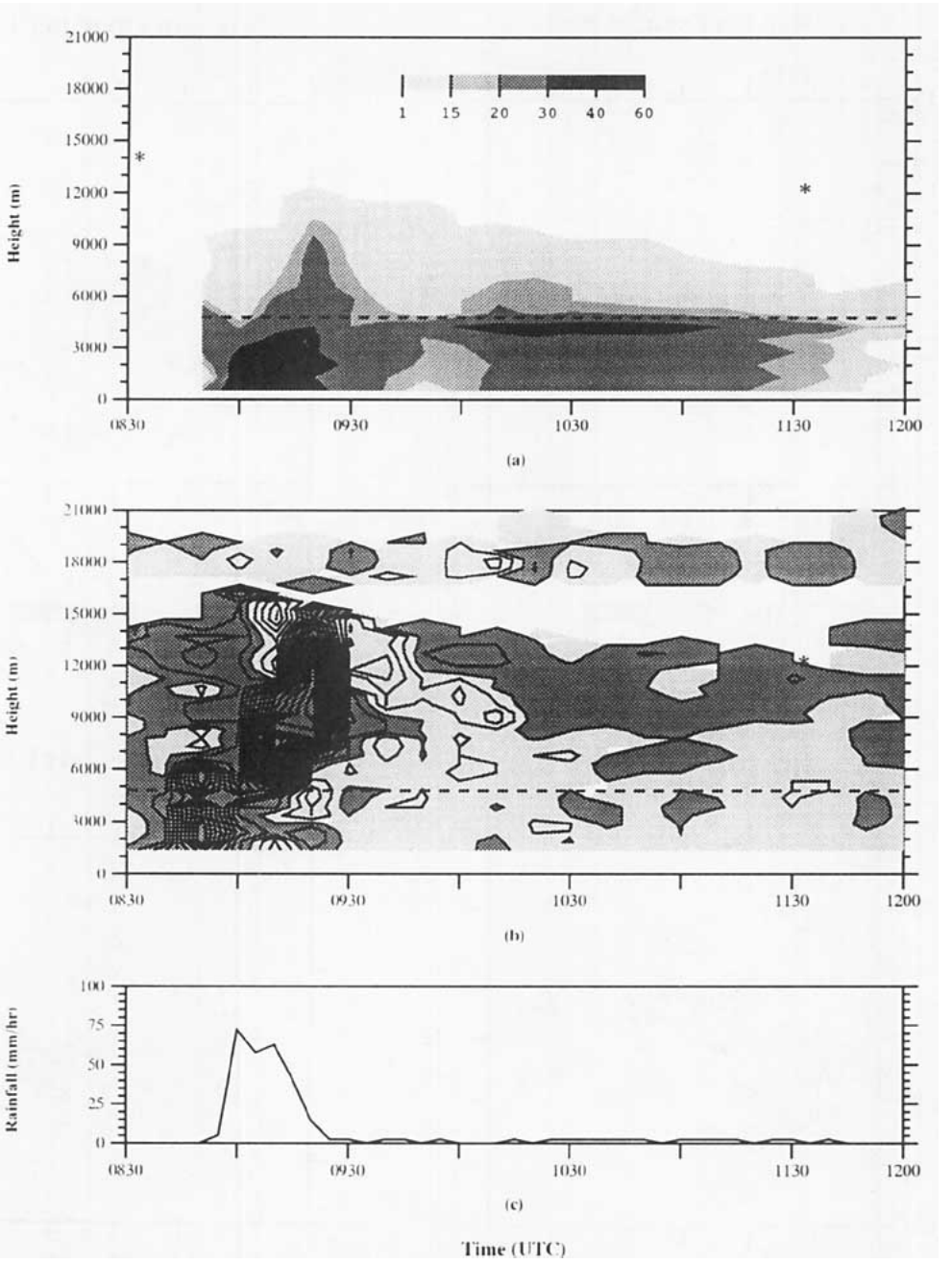

FIG. 7. Time–height cross sections for the 5 December 1989 MCS. (a) Radar reflectivity from the MIT radar data over the location of the wind profiler [adapted from Williams and Ecklund (1992)]. Values are in dBZ. Contour interval is shown by gray scale at top of plot. (b) Vertical velocity, from the wind profiler data. Regions of upward motion denoted by dark shading and downward motion by light shading. Contour interval is 0.5 m s^{-1}. (c) Surface rainfall measured at the Berrimah raingauge site (approximately 4 km west of the wind profiler site). Units are millimeters per hour. In (a), (b), and (c) horizontal axis is time (UTC). In (a) and (b) asterisks denote approximate cloud-top height based on GMS data, and the dashed horizontal lines indicate the melting level.

The time series of rain accumulation shows that this period was characterized by very light rain.

After about 1010 UTC, upward motion was present in the middle to upper troposphere, with mesoscale downward motion at lower levels. This upward motion coincided with the development of a distinct maximum in radar reflectivity (bright band) near the melting level. The low-level reflectivity pattern (Fig. 8d) indicates the development of more widespread stratiform precipitation over the profiler at this time. The magni-

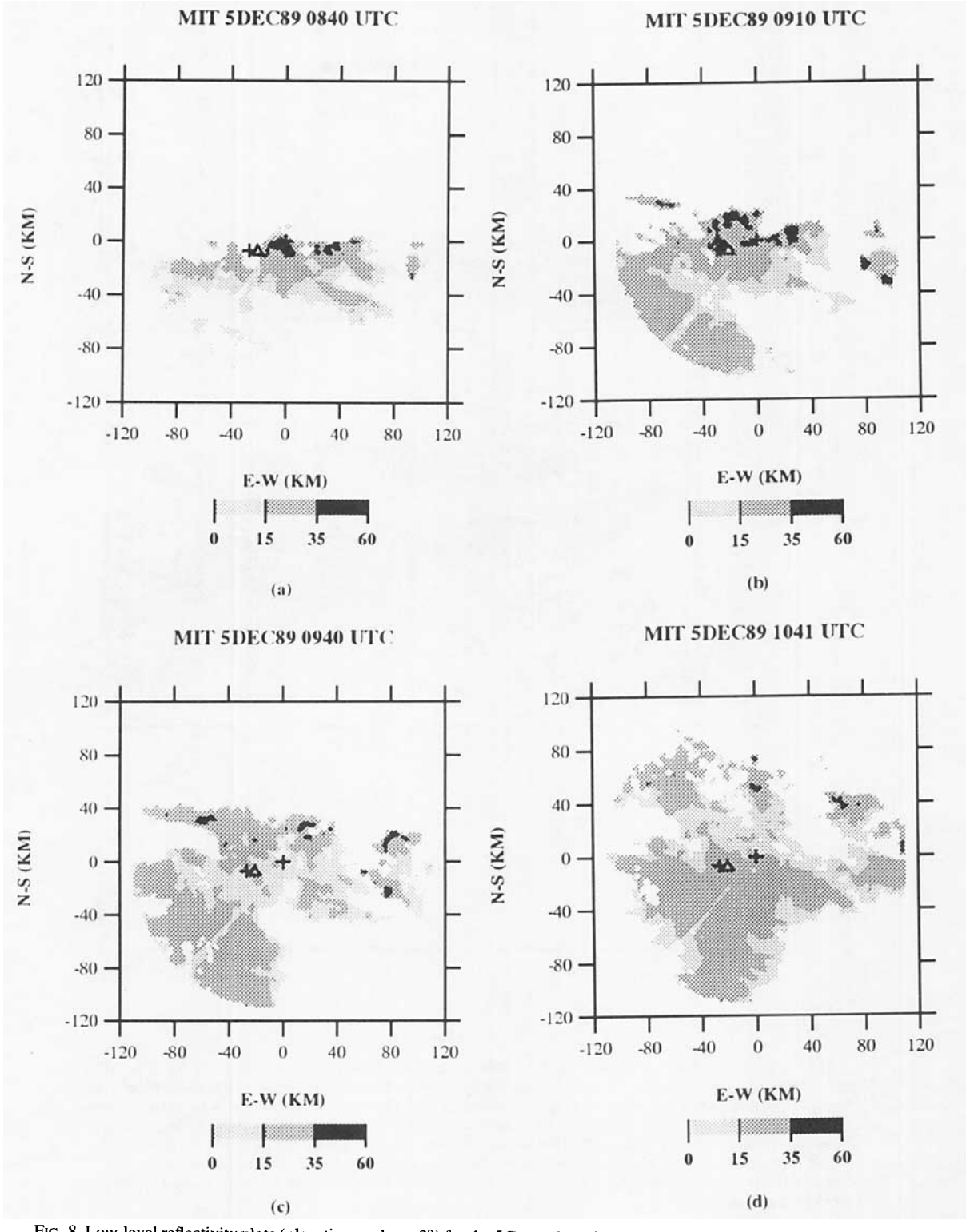

FIG. 8. Low-level reflectivity plots (elevation angles <2°) for the 5 December 1989 MCS centered on the MIT radar. Reflectivity scale (dBZ) is shown below each plot. Location of the radars is indicated by the plus symbols. Triangle denotes the location of the wind profiler.

tudes of motion in the stratiform region are generally weak, ranging up to about 0.5 m s^{-1}.

The reflectivity cross section in Fig. 7a shows a cessation of the bright band after about 1110 UTC. The reduction in the bright band appears to be related to enhanced subsidence occurring in the stratiform region at this time. The precipitation intensity remained very light throughout the duration of the stratiform region in the vicinity of the profiler. During the observational period, a total of 25.2 mm of rain was recorded at the Berrimah raingauge, with 85% occurring in association with the passage of the convective region.

2) 12 JANUARY 1990

The 0000 UTC 12 January 1990 Darwin sounding is shown in Fig. 9. The plot shows nearly saturated conditions from the surface to 450 mb. The temperature profile indicates only a small departure from moist-adiabatic conditions over a deep layer of the troposphere, which is characteristic of the monsoon regime (Keenan and Rutledge 1993). Deep northeasterly flow extending from the surface up to 200 mb is evident in the wind profile. In this case, it is likely that the low-level winds were modified by previous convection on this day (see below). Holland (1986) associated monsoon conditions in Darwin with west to northwest flow at 850 mb.

The 12 January 1990 MCS (hereafter referred to as 12Jan90) consisted of a monsoonal rainband with an associated stratiform region that formed in a low-CAPE, low-shear environment (Keenan and Rutledge 1993). The system formed as one of several monsoon bands north of Darwin. Prior to the observational period that we describe, several of these bands passed over the Darwin area. The rainband and associated stratiform region we studied moved onshore toward the south-southeast across the Darwin area and then merged with cells forming along a sea-breeze front east of Darwin. The convective band passed over the radar baseline at approximately 0845 UTC. Convective towers reached heights of about 12 km. A large stratiform region developed in a northeast–southwest orientation over Darwin, which moved at about 5.5 m s^{-1} toward the southeast.

The evolution of the 12Jan90 monsoon case has been previously described by Keenan and Rutledge (1993) using dual-Doppler analysis and can serve as a basis of comparison for this study. Time–height cross sections of vertical velocity and reflectivity over the profiler for the 12Jan90 monsoon case are shown in Fig. 10. Low-level horizontal reflectivity plots are shown in Fig. 11. Because the MIT radar was collecting only surveillance data (low-level PPIs) prior to 1010 UTC, the reflectivity cross section (Fig. 10a) was constructed using MIT data from 1010 UTC to the end of analysis, and TOGA radar data prior to 1010 UTC. As stated previously, cross-section analysis using TOGA data was performed

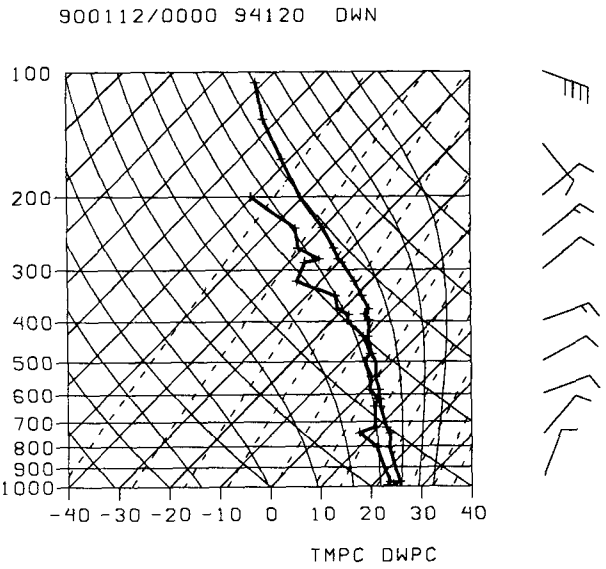

FIG. 9. Same as in Fig. 6 except for 0000 UTC 12 January 1990.

approximately 20 km east of the profiler location, along the radar baseline. Due to instrument problems, rainfall data from the Berrimah site were not available on this date. In Fig. 10c, we show rainfall data from the Koolpinyah raingauge, coincident with the MIT radar site. Data from this raingauge roughly correspond to the location of the reflectivity cross section prior to 1010 UTC.

Inspection of Fig. 10b shows a distinctly different vertical motion structure compared to the monsoon-break case, as a series of updraft regions (bands) crossed over the profiler during the passage of this system. The strength of the updrafts progressively decreased from about 2–3 m s^{-1} in the first band (0830–0920 UTC) to less than 0.5 m s^{-1} in the last band (1100–1200 UTC). The magnitude of the peak updraft is in reasonable agreement with previous studies of oceanic convection (LeMone and Zipser 1980; Zipser and LeMone 1980; Jorgensen and LeMone 1989; Webster and Houze 1991). Each of these ascent regions was separated by relatively narrow (about 20-minute timescale) regions of subsidence. The magnitude of this downward motion was fairly constant, being less than 0.5 m s^{-1} throughout the sampling period. Moreover, with the exception of the earliest observational time (0830 UTC), subsidence occurred at low levels throughout the observational period. This low-level subsidence region became progressively deeper with time. Note that the vertical velocities in Fig. 10b extend several kilometers above the satellite-derived cloud-top heights. The reason for the discrepancy is not apparent; however, it may be related to the relatively large echo-top gradients observed in the radar data.

The magnitude of vertical velocities sampled by the wind profiler is in reasonable agreement with dual-

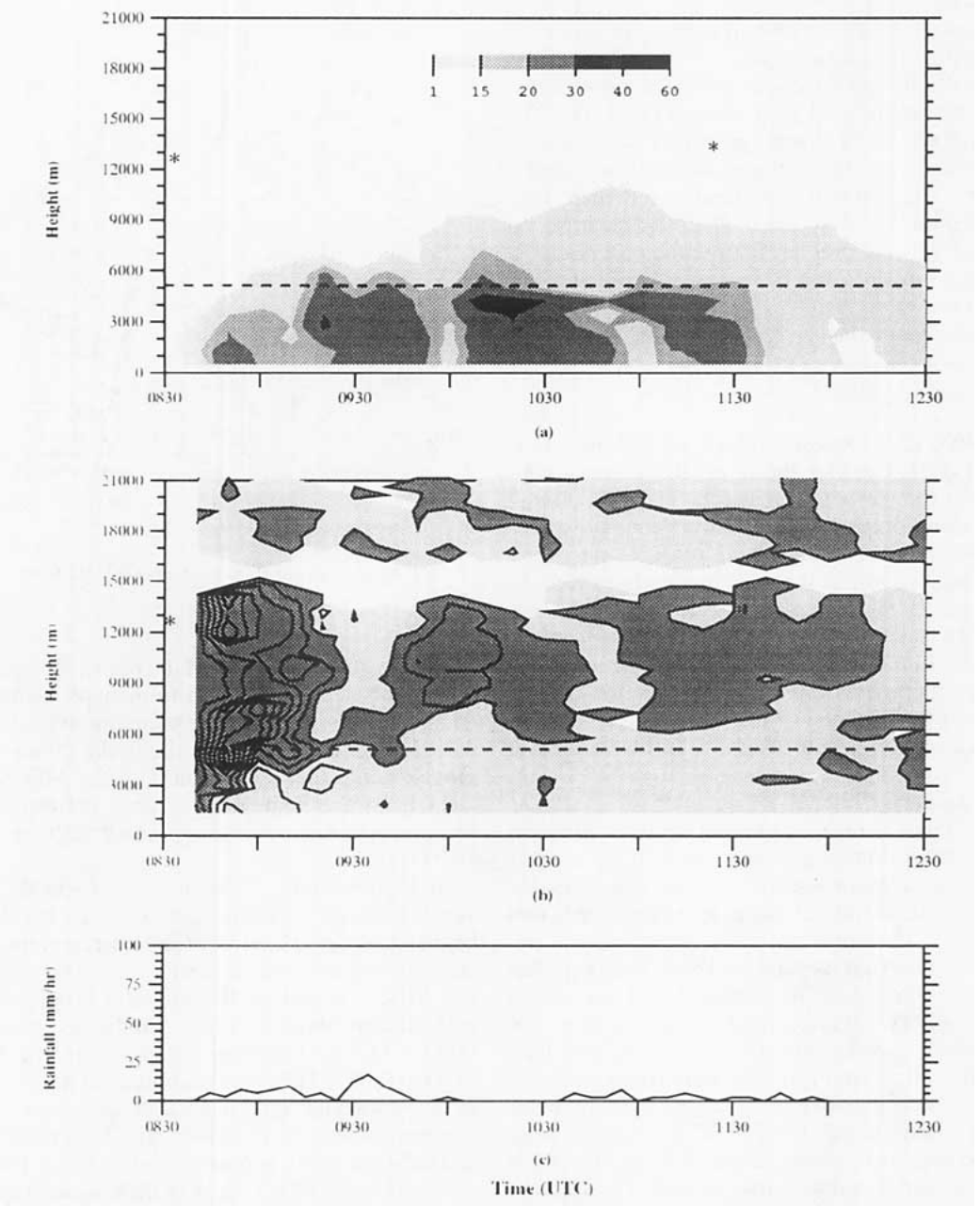

FIG. 10. As in Figs. 7a–c except for the 12 January 1990 MCS. Time–height cross section of reflectivity measured with (a) the TOGA radar at a point 20 km east of the profiler prior to 1010 UTC and (b) with MIT radar data over the location of the wind profiler after 1010 UTC. Surface rainfall in (c) measured at the Koolpinyah raingauge site (approximately 23 km east of the wind profiler site).

Doppler-derived vertical velocities reported in Keenan and Rutledge (1993) at 1010 UTC (see their Figs. 9 and 12). Their results showed a series of convective bands in the stratiform region oriented parallel to the direction of storm motion, which they attributed to convective-scale overturning. This interpretation is consistent with the vertical velocity field presented in this study.

The reflectivity cross section prior to 1010 UTC (constructed with TOGA data) shows a very limited vertical extent of the MCS, which is in contrast to the vertical motion field sampled by the wind profiler. The low echo tops seen in the reflectivity cross section (Fig. 10a), when compared with the depth of vertical velocity prior to about 1000 UTC (Fig. 10b), suggest differences in storm intensity along the radar baseline.

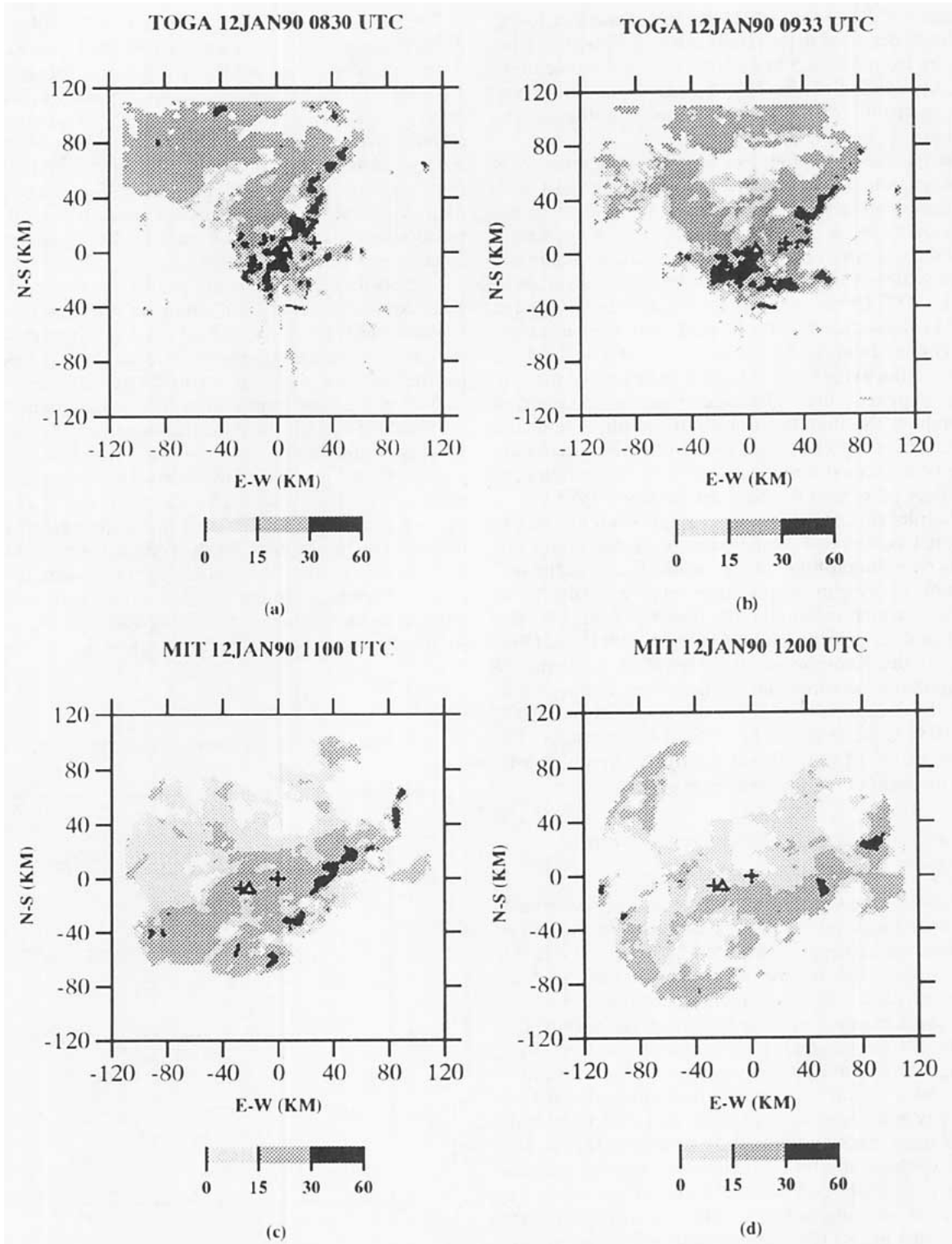

FIG. 11. As in Fig. 8 except for the 12 January 1990 MCS. Note that plots (a) and (b) are centered on the TOGA radar, and plots (c) and (d) are centered on the MIT radar. Some of the high reflectivity values in the vicinity of the TOGA radar in (a) and (b) are ground clutter targets.

Keenan and Rutledge (1993) noted that sharp echo-top gradients occurred in the stratiform region, with heights ranging from 6.5–8.5 to 11.5 km over a distance of 40 km. Attenuation of the TOGA radar beam could also be responsible for the relatively low echo-top heights seen in Fig. 8a.

Despite the anomalous low echo tops, the reflectivity cross section shows a series of convective cells with reflectivity values ranging from 20 to 30 dBZ, separated by a region of lower reflectivities, in agreement with the overall vertical velocity structure. Maximum reflectivities of 30–40 dBZ occurred near 3 km at about 0920 UTC. Cross sections in Keenan and Rutledge (1993) show that the 20–30-dBZ contour was generally confined to heights below about 5–6 km. That the largest reflectivities were found at or below the melting level suggests that glaciated conditions occurred throughout the middle to upper troposphere and that the vast majority of precipitation from this system may have been formed through a low-level warm rain (coalescence) process (Keenan and Rutledge 1993).

The plot of rainfall intensity at the Koolpinyah site does not correspond to the passage of maximum updrafts over the profiler. This is probably due to the orientation of system propagation relative to the radar baseline, which resulted in the bands passing over the wind profiler prior to passing over the MIT site (Fig. 11). At the Koolpinyah site, a total of 10.8 mm of precipitation occurred during the observation period. With the exception of a half-hour period between 1005 and 1035 UTC in which no rainfall was recorded, the accumulation of rainfall was relatively evenly distributed throughout the observational period.

b. *Composite analysis of break regime vertical motion*

In addition to the 5Dec89 case previously described, the other break period MCSs analyzed in this study occurred on 22 January 1990 and 28 January 1990. All three of the break regime MCSs had similar structural characteristics: a leading line of convection with intense precipitation and sharp horizontal reflectivity gradients; a zone of weaker reflectivities and very light precipitation immediately to the rear of the convective line; and a region with relatively small horizontal reflectivity gradients, light rainfall, and a characteristic bright band marking the trailing stratiform region. Because of these similar characteristics, the vertical motion profiles in the convective, transition, and stratiform regions were composited in order to characterize the salient features of the vertical motion field in each region. It should be noted that all systems described herein were sampled during the mature to dissipating stages of convective activity [stages defined by Leary and Houze (1979)]. Therefore, the resulting composite profiles may not be applicable to earlier stages of the MCS life cycle.

The categorization of vertical velocity profiles into discrete system regimes (convective, transition, stratiform) is somewhat subjective because of limited amounts of data and the evolution of each MCS as it moved over the profiler. In this study, a combination of reflectivity and surface rainfall characteristics were used to identify the convective, transition, and stratiform regions of each break regime MCS over the profiler. A composite analysis is obviously not available for monsoon cases since we examined only one monsoon case in this study.

Composite vertical velocity profiles of the break regime convective, transition, and stratiform regions are shown in Fig. 12. A total of 19 averaged spectra were used to construct a composite field of vertical motion for the convective region, 13 in the transition region, and 37 in the stratiform region. Error bars, indicating the standard deviation around the mean, are also shown for each profile in Fig. 12. Note that these estimates are presented only at selected locations where the curve-fit program was least affected by spectra merging (lower troposphere for stratiform and transition region profiles, middle troposphere for the convective region profile). In this section, we restrict our discussion to tropospheric vertical motion profiles. Analysis of vertical motions in the vicinity of the tropopause and the lower stratosphere will be presented in section 5.

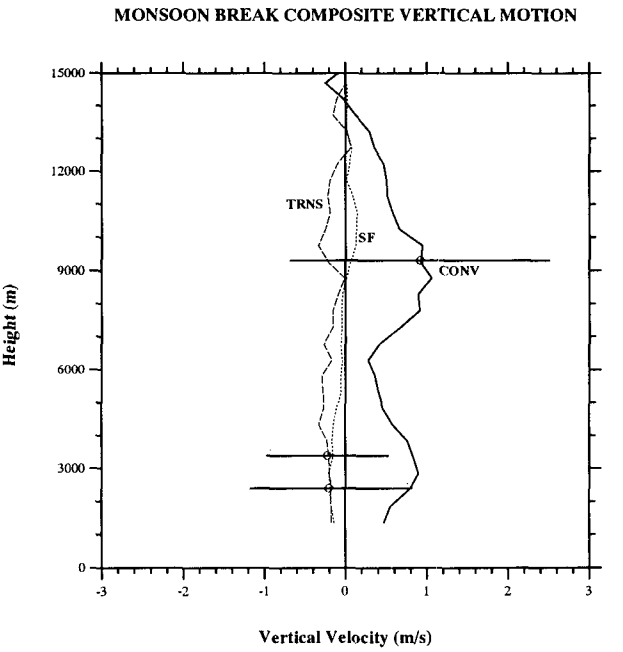

FIG. 12. DUNDEE composite vertical motion (m s^{-1}) profiles in the convective (solid), transition (long-dashed), and stratiform (short-dotted) regions based on wind profiler data from the three monsoon-break period cases discussed in text. Horizontal lines indicate standard deviation based on the results of the curve-fit algorithm.

The vertical motion composite profile in the convective region (Fig. 12) shows upward motion throughout the depth of the troposphere, except near the tropopause. As mentioned previously, the large dispersion in the vertical velocity estimates are indicative of large turbulence and resulting broad spectra. Two levels of maximum ascent are evident, a low-level peak centered near 3 km and a second peak in the middle troposphere. All three of the monsoon break MCSs were characterized by this bimodal updraft structure, which persisted for several hours while the systems were sampled. The low-level peak was associated with convective elements forming along the leading edge of the convective line. This low-level upward motion evidently drove a warm rain coalescence process, which was responsible for brief but heavy rain rates coincident with the leading edge of each break regime MCS studied. The upper-ascent peak was associated with deep, mature convective elements behind the leading edge of the squall line. Precipitation processes in this deep updraft were evidently associated with mixed phase processes, based on vertical reflectivity profiles.

The DUNDEE transition region vertical motion composite shows descending motion throughout almost the entire troposphere (Fig. 12). The descent has a double-peak structure with maxima located near 10 and 4.3 km. Similar downdraft structures have been documented in previous studies of tropical and middle latitude convection (Heymsfield and Schotz 1985; Chalon et al. 1988; Biggerstaff and Houze 1993). Heymsfield and Schotz (1985) have shown that the upper-level subsidence is a result of the dynamical interaction of the convective outflow (front-to-rear storm-relative flow) near cloud top with the ambient wind field. Cross sections of storm-relative horizontal flow shown in Petersen (1992) for each of the three MCSs we studied indicate convergence of front-to-rear flow to the rear of the convective line and suggest that this mechanism may be operating in the DUNDEE squall lines we describe. The low-level descent is likely associated with water loading, as well as cooling from melting and evaporation (Biggerstaff and Houze 1993).

The DUNDEE composite profile for the stratiform region (Fig. 12) shows subsidence in the middle to lower troposphere with a maximum near 3 km. The crossover from descent to ascent occurred near 8.8 km; however, due to the relatively large dispersion in the clear-air estimates and the existence of spectra merging in this region (see discussion in section 2), the location of the crossover level in the profile is not deemed significant. Ascending motion was found in the upper troposphere with a maximum centered near 10.8 km.

In Figs. 13–15, we compare the DUNDEE vertical motion profiles with similar profiles from different geographic regions. Although such a comparison is complicated by differences in observational techniques, MCS life cycle stage, and the large variation in spatial scales utilized in these studies, the results are presented in order to place the DUNDEE profiles in the context of similar profiles derived from other tropical and middle latitude locations. Moreover, due to the large dispersion in the DUNDEE vertical velocity estimates, our purpose here is only to compare the salient features in the profiles.

Composite vertical motion profiles from convective region MCSs are shown in Fig. 13. This figure includes profiles derived from eastern Atlantic tropical oceanic squall lines using rawinsonde and aircraft data (Houze and Rappaport 1984; Gamache and Houze 1985), a West African tropical continental MCS using dual Doppler radar analysis (Chong et al. 1983), a composite of tropical western Pacific island MCSs using wind profiler data (Balsley et al. 1988), and a middle latitude MCS using dual–Doppler radar analysis (Biggerstaff and Houze 1993). The double-peak structure of the DUNDEE composite shown in Fig. 13 is similar to convective vertical velocity profiles of the tropical oceanic squall lines analyzed by Gamache and Houze (1985) and Houze and Rappaport (1984) in GATE. The GATE profiles show a low-level peak centered near 2–3 km and an upper peak centered near 8 km; however, the magnitude of the peak vertical motion in the GATE profiles was significantly less than the DUNDEE composite peak vertical motion values presented in this study.

The vertical motion profiles from both the tropical West Africa and middle latitude MCSs show a single upward motion peak in the middle troposphere with magnitudes on the order of 1–2 m s^{-1} (Fig. 13). In the western Pacific (Pohnpei Island), the composite profile shows a single ascent peak (1.8 m s^{-1}) in the upper troposphere. In particular, the peak ascent in the west Pacific composite is situated several kilometers above the corresponding peak in the DUNDEE profile. It is not possible to determine whether an ascent peak exists in the lower troposphere at Pohnpei Island due to the restriction of sampling above about 3.5 km. Both the DUNDEE and west Pacific composite show a region with mostly subsidence in the upper troposphere; however, the base of the subsidence region in DUNDEE occurred about 2 km below the corresponding base in the Pohnpei profile (Fig. 13), even though the height of the tropopause in the two regions is similar (17 km).

In Fig. 14, we compare the DUNDEE transition zone composite with similar profiles from middle latitude MCSs using dual Doppler radar (Smull and Houze 1987; Biggerstaff and Houze 1993), a West African tropical continental squall line using dual Doppler radar (Chalon et al. 1988), and a GATE tropical oceanic system using composited rawinsonde data (Houze and Rappaport 1984). The results all show subsidence below the melting level; however, some of the profiles (Houze and Rappaport 1984; Smull and Houze 1987) show ascending motion in the middle to upper troposphere while the others, including the DUNDEE com-

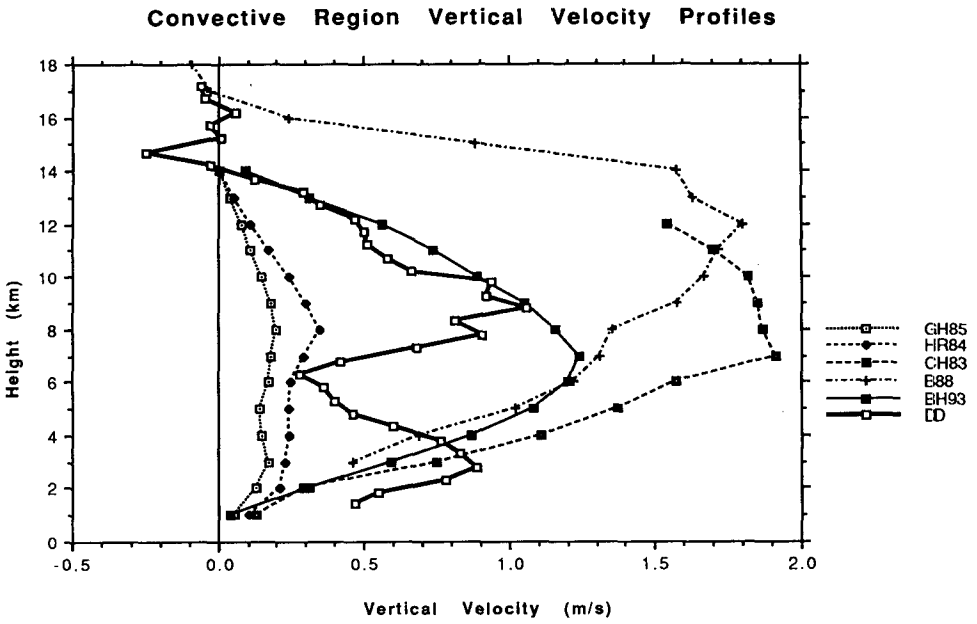

FIG. 13. Comparison of convective region vertical motion profiles. Symbols in legend refer to the following: GH85 for Gamache and Houze (1985); HR84 for Houze and Rappaport (1984); CH83 for Chong et al. (1983) [adapted from Houze (1989)]; B88 for Balsley et al. (1988); BH93 for Biggerstaff and Houze (1993); and DD for the DUNDEE results of this study. Note that widely different sample sizes and temporal and spatial averaging go into the various curves of this figure (see text for details).

posite, show descending motion throughout this region. The reason for the discrepancy between the profiles above the melting level is not readily apparent but may be related to the subjectivity involved in defining the transition zone region.

In Fig. 15, we show the DUNDEE stratiform composite compared to similar profiles from the western Pacific (Pohnpei Island) using composited wind profiler data (Balsley et al. 1988), the South China Sea using composited ship rawinsonde data (Johnson 1982), a West Africa continental tropical MCS using the single–Doppler radar (VAD) retrieval (Chong et al. 1987), a tropical oceanic system in the east Atlantic using rawinsonde and aircraft data (Houze and Rappaport 1984), and a middle latitude MCS using the single–Doppler radar (EVAD) retrieval technique (Rutledge et al. 1988). The profiles all indicate descent in the lower troposphere and ascent in the upper troposphere, with magnitudes ranging up to 0.5 m s^{-1}. The magnitude of the mesoscale downdraft is by far strongest in the middle latitude case.

In the upper troposphere, the DUNDEE stratiform composite profile (Fig. 15) is similar to the composite profile for stratiform rain obtained by Balsley et al. (1988). Both composite profiles show a primary ascent peak in the stratiform region centered near 10–11 km, a secondary peak centered near cloud top (12.5 km in the DUNDEE composite and about 14 km in the Pohnpei composite), and a region of subsidence extending upward from cloud top to the vicinity of the tropopause. The subsidence layer in the vicinity of the tropopause has also been diagnosed for a middle latitude MCS by Johnson et al. (1990). In their study, Johnson et al. argued that the subsidence was due primarily to downward sloping isentropes to the rear of the convective line and was independent of radiative effects. Although the composite DUNDEE profile shows subsidence in the vicinity of the tropopause, it should be noted that the vertical motion at various times in this region was upward (see Fig. 7). The oscillatory nature of the vertical drafts suggests that the motion may have been associated with gravity waves forced by deep convection. This phenomena will be further described in section 5.

c. *Composite analysis of break regime surface rainfall*

The surface raingauge network was utilized in conjunction with low-level radar reflectivity plots to correlate rainfall amounts in the convective and stratiform regions of the three monsoon-break systems. There were over 30 raingauges collecting surface rainfall data for the 1989/90 DUNDEE season (T. Keenan 1993, personal communication); however, we only used gauges where the delineation of the convective, transition, and stratiform regions could be determined with low-level reflectivity data. Also, some gauges were not collecting data for the time periods of interest. Thus, the total number of raingauges used to determine the

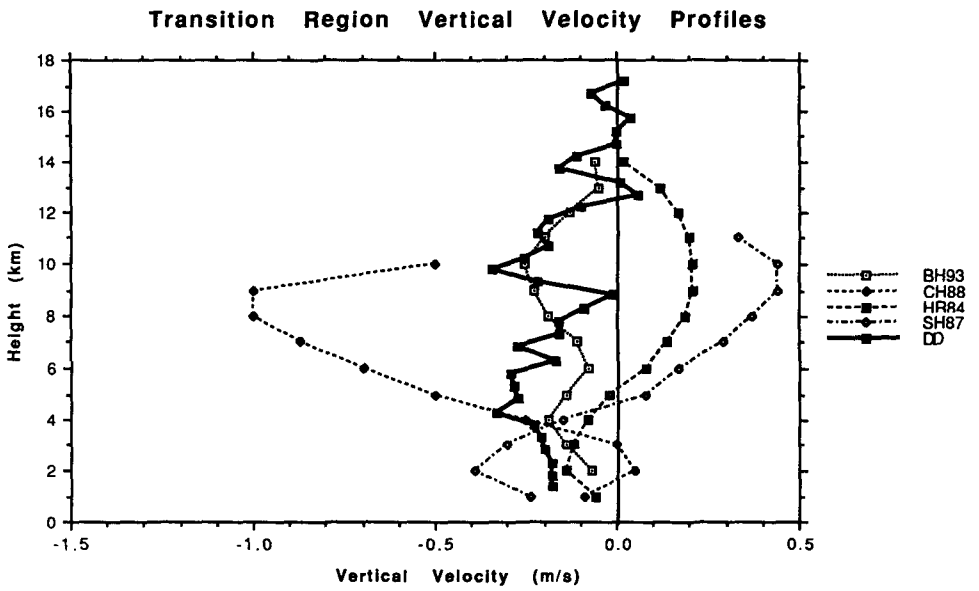

FIG. 14. Comparison of transition region vertical motion profiles. Symbols in legend refer to the following: BH93 for Biggerstaff and Houze (1993); CH88 for Chalon et al. (1988); HR84 for Houze and Rappaport (1984); SH87 for Smull and Houze (1987); and DD—DUNDEE results of this study. Note that widely different sample sizes and temporal and spatial averaging go into the various curves of this figure (see text for details).

rainfall characteristics of each monsoon break MCS varied from 15 to 17. Although this procedure eliminated a significant number of potential data points, no assumptions of steady-state conditions were used to determine rainfall during the passage of the MCS over a particular gauge.

The analysis of rainfall distribution in each region of the monsoon-break MCSs indicates that a significant

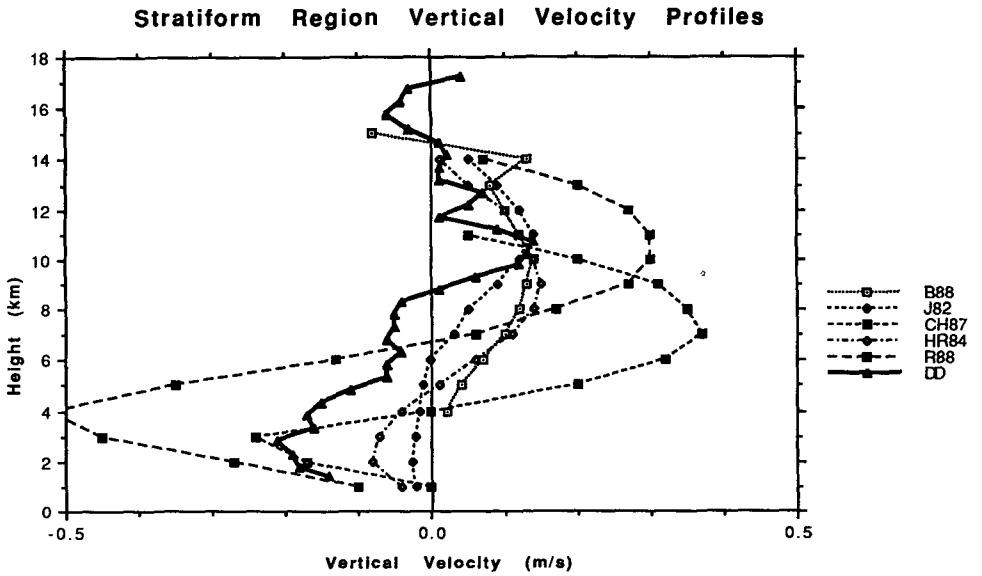

FIG. 15. Comparison of stratiform region vertical motion profiles. Symbols in legend refer to the following: B88 for Balsley et al. (1988); J82 for Johnson (1982); CH87 for Chong et al. (1987); HR84 for Houze and Rappaport (1984); R88 for Rutledge et al. (1988); and DD for the DUNDEE results of this study. Note that widely different sample sizes and temporal and spatial averaging go into the various curves of this figure (see text for details).

portion of the total rainfall (71%–80%) was associated with the passage of the convective line. Only small amounts of rainfall (<5% of the total) were recorded during the passage of the transition zone. The high proportion of convective rainfall is in agreement with Simpson et al. (1993), who diagnosed convective and stratiform rainfall contributions from three island-generated MCSs, which occurred over Melville and Bathurst Islands during the monsoon break. In their study, Simpson et al. (1993) used a radar Z–R relationship to calculate rainfall totals and found that roughly 92% of the total rainfall was associated with the convective portion of the MCSs. The contribution of stratiform rainfall in both the Simpson et al. and DUNDEE studies (17%–28%) is less than the amount diagnosed by Houze (1977) for GATE squall line systems (40%).

The raingauge data were also scrutinized to determine whether the convective region bimodal precipitation peak sampled at the Berrimah raingauge site during the passage of the 5Dec89 MCSs was also present at other locations along the convective line of all three break monsoon systems. The results (not shown) indicated that the vast majority of the gauges in the three monsoon-break MCSs showed a distinct bimodal or multimodal rainfall peak separated in time by 10–30 min. Moreover, in most cases the first peak (in time) had the largest magnitude of rainfall intensity. The results support the notion that these MCSs were multicellular and also suggest that warm rain coalescence processes, characteristic of the first rainfall peak, played a significant role in contributing to the total surface rainfall and latent heating produced by the systems.

5. Vertical motion at the tropopause

Clear-air vertical motion in the vicinity of the tropopause (≈16.5–17.5 km) was detected by the wind profiler throughout the MCS life cycle of all the systems we studied (Figs. 7 and 10). As discussed by Fovell et al. (1992), gravity wave forcing at the tropopause is an important source of momentum transfer from the troposphere into the stratosphere and can influence the mean flow in the middle atmosphere. In general, the vertical drafts were detected from within about one kilometer below the tropopause upward into the lower stratosphere. The motion in this region oscillated between ascent and descent both as a function of altitude and time, suggesting a gravity wave origin. Moreover, the period of oscillation displayed a large range of variation within each MCS, with horizontal periods ranging from 0.3 to 1.3 h. The vertical wavelength appeared to vary between 2 and 4 km. However, restrictions in the extent of vertical sampling did not allow for accurate estimates of the vertical wavelength in most instances. Although the magnitude of this motion was generally less than 0.5 m s^{-1}, oscillations in excess of 1 m s^{-1} were sampled in all three of the break regime MCSs.

It should be noted that the vertical velocity estimates in the vicinity of the tropopause and lower stratosphere may be contaminated as a result of aspect sensitivity effects. As described previously in section 2, aspect sensitivity occurs when refractive layers are inclined with respect to the horizontal plane. This situation allows for a component of the horizontal wind to be resolved with the true vertical velocity. The effect appears to be most pronounced for radars operating at VHF in hydrostatically stable regions of the atmosphere (i.e., tropopause–lower stratosphere), since these radars are sensitive to quasi-specular reflection from stably stratified refractive layers (Gage 1990). Since the Darwin profiler was operated in vertical pointing mode only, it is impossible to quantify this potential source of error.

6. Conclusions

We have discussed the vertical velocity structure in several tropical MCSs that passed over Darwin, Australia, during the 1989/90 DUNDEE field season, based on analysis of wind profiler data. In particular, we have analyzed the details of vertical motion, radar reflectivity, and surface rainfall structures in one monsoon-break MCS and one monsoon regime MCS.

The monsoon-break MCS was characterized by a leading line of convection, a reflectivity trough immediately to the rear of the line, and a trailing stratiform precipitation region, similar to many previous studies of both tropical and middle latitude MCSs. The MCS was in its mature to dissipating stage by the time it crossed the observational network. The wind profiler sampled coexisting updraft cores in the convective region that crossed the profiler over a period of approximately 30 min. The initial updraft core was centered in the lower troposphere (near 3 km) and was followed by a deeper updraft, centered in the middle troposphere (near 9 km). The orientation of these updraft cores was due to the rearward tilt and multicellular nature of the convection as it crossed the observational network. Based on individual raingauges and rainfall data from a network of gauges, the break regime MCS had peaks in surface rainfall intensity corresponding to the passage of both low- and upper-level updrafts. Furthermore, the rainfall rate peaks were comparable in magnitude, indicating that warm rain coalescence processes (associated with the low-level updraft peak) were as important to precipitation production as mixed phase processes involving both ice and supercooled water (associated with the upper-level updraft peak). Approximately 85% of the total rainfall measured by a nearby surface raingauge network was associated with the passage of the convective region. Immediately to the rear of the convective line, the profiler sampled deep subsidence on the order of 1–2 m s^{-1}. Vertical motion in the stratiform region rarely exceeded 1 m s^{-1}.

The monsoon case showed a different vertical velocity structure than the break system. The monsoonal MCS was characterized by a series of convective bands that passed over the profiler during the sampling period. Both the updraft strength and depth became weaker with the passage of each band. The monsoon MCS could be characterized as stratiform precipitation with embedded convection, consistent with other studies on monsoon convection in the vicinity of Darwin (e.g., Houze 1989; Keenan and Carbone 1992; Mapes and Houze 1992). Surface rainfall data for the monsoon case were not available within the immediate vicinity of the profiler site; however, data collected at the MIT radar location suggested that the distribution of rainfall was more uniform during the observational period than in the monsoon-break cases.

Two additional break regime cases were also analyzed in their mature to dissipating life cycles and found to have similar reflectivity, vertical velocity, and precipitation characteristics to the previously described monsoon-break MCS. Composite vertical motion profiles were generated for the convective, transition, and stratiform regions of all three monsoon-break cases. In the convective region, a double-peaked ascent profile was shown with peaks located near 3 and 9 km. The composite profile in the transition zone showed subsidence throughout the majority of the troposphere with dual peaks of comparable magnitude at upper and lower levels. In the stratiform region, the DUNDEE composite showed descending motion occurring below about 8.5 km with a peak near the melting level and a double-peak ascent structure in the upper troposphere.

All three of the DUNDEE monsoon-break cases showed significantly smaller contributions by stratiform rain to the total rain accumulation when compared to studies of MCSs in other tropical locations (i.e., GATE). The stratiform region did not contribute more than 28% to the total rainfall in any of the three monsoon-break systems we studied.

The composite DUNDEE vertical velocity profiles were compared with similar profiles from other geographic regions. Although differences in sampling techniques, life cycle stage, and spatial scales precluded detailed comparisons, the DUNDEE composites were found to have similarities to both middle latitude and tropical MCSs. In particular, the double-peak structure in the convective region is similar to corresponding vertical velocity profiles of GATE tropical oceanic squall lines. In the transition zone, the DUNDEE composite profile is consistent with the vertical velocity structure shown in the transition zone of a COPT 81 West African squall line described by Chalon et al. (1988) and a midlatitude squall line discussed by Biggerstaff and Houze (1993). The DUNDEE composite in the stratiform region also exhibited similarities to previous studies of both tropical and middle latitude MCSs.

Clear-air vertical motion was sampled by the profiler in a region extending from near the tropopause into the lower stratosphere. The motions displayed oscillations between ascent and descent during the passage of each MCS, suggesting a gravity wave origin, probably forced by the occurrence of convective updrafts impinging on the tropopause. The horizontal wave period varied from 0.3 to 1.3 h. The random variation of wave structure may have been caused by a superposition of waves from numerous convective elements impinging on the tropopause in the vicinity of the monsoon trough.

Acknowledgments. Drs. Ken Gage, Warner Ecklund, and Mike Manton played key roles in establishing the Darwin profiler site. Doug Burks and Takmeng Wong of CSU assisted in the data analysis. Dr. Anthony Riddle of the NOAA Aeronomy Laboratory assisted in the interpretation of wind profiler spectra data. Drs. T. Keenan and P. May of BMRC also made important contributions to this research. DUNDEE was enhanced by facilities deployed for NASA's TRMM Ground Truth Program in Darwin under the direction of Otto Thiele. The authors would like to thank Dr. Ed Zipser and two anonymous reviewers for their constructive comments. This work was supported by Grant ATM-9015485 from the National Science Foundation and Contract NA90RAH00077 from NOAA (Office of Global Programs—TOGA COARE).

REFERENCES

Adler, R. F., and M. J. Markus, 1982: Determination of thunderstorm heights and intensities from GOES infrared data. Preprints, *Ninth Conf. on Weather Forecasting and Analysis,* Seattle, Amer. Meteor. Soc., 250–257.

Balsley, B. B., W. L. Ecklund, D. A. Carter, A. C. Riddle, and K. S. Gage, 1988: Average vertical motions in the tropical atmosphere observed by a radar wind profiler on Pohnpei (7°N latitude, 157°E longitude). *J. Atmos. Sci.,* **45,** 396–405.

Biggerstaff, M. I., and R. A. Houze, Jr., 1993: Kinematics and microphysics of the transition zone of the 10–11 June 1985 squall line. *J. Atmos. Sci.,* **50,** 3091–3110.

Carter, D. A., W. L. Ecklund, J. R. McAfee, K. S. Gage, T. Keenan, and M. Manton, 1991: Results from the first year of observations using the Darwin VHF wind profiler. Preprints, *25th Int. Conf. on Radar Meteorology,* Paris, France, Amer. Meteor. Soc., 288–291.

Chalon, J. P., G. Jaubert, F. Roux, and J. P. Lafore, 1988: The West African squall line observed on 23 June 1981 during COPT 81: Mesoscale structure and transports. *J. Atmos. Sci.,* **45,** 2744–2763.

Chilson, P. B., C. W. Ulbrich, M. F. Larsen, P. Perillat, and J. E. Keener, 1993: Observations of a tropical thunderstorm using a vertically pointing, dual-frequency, collinear beam Doppler radar. *J. Atmos. Oceanic Technol.,* **10,** 663–673.

Chong, M., J. Testud, and F. Roux, 1983: Three-dimensional wind field analysis from dual-Doppler radar data. Part II: Minimizing the error due to temporal variation. *J. Climate Appl. Meteor.,* **22,** 1216–1226.

——, P. Amayenc, G. Scialom, and J. Testud, 1987: A tropical squall line observed during the COPT 81 experiment in West Africa. Part I: Kinematic structure inferred from dual-Doppler radar data. *Mon. Wea. Rev.,* **115,** 670–694.

Clark, W. L., and D. A. Carter, 1980: Real-time scaling of atmospheric parameters from radars using the MST technique. Preprints, *19th Conf. on Radar Meteorology,* Miami Beach, FL, Amer. Meteor. Soc., 599–604.

DeMaria, M., 1985: Linear response of a stratified tropical atmosphere to convective forcing. *J. Atmos. Sci.,* **42,** 113–121.

Fovell, R., D. Durran, and J. R. Holton, 1992: Numerical simulations of convectively generated stratospheric gravity waves. *J. Atmos. Sci.,* **49,** 1427–1442.

Gage, K. S., 1990: Radar observations of the free atmosphere: Structure and dynamics. *Radar in Meteorology,* D. Atlas, Ed., Amer. Meteor. Soc., 534–565.

Gamache, J. F., and R. A. Houze Jr., 1985: Further analysis of the composite wind and thermodynamic structure of the 12 September GATE squall line. *Mon. Wea. Rev.,* **113,** 1241–1259.

Hack, J. J., and W. H. Schubert, 1990: Some dynamical properties of idealized thermally forced meridional circulations in the tropics. *Meteor. Atmos. Phys.,* **44,** 101–117.

Hartmann, D. L., H. H. Hendon, and R. A. Houze Jr., 1984: Some implications of the mesoscale circulations in tropical cloud clusters for large-scale dynamics and climate. *J. Atmos. Sci.,* **41,** 113–121.

Heymsfield, G. M., and S. Schotz, 1985: Structure and evolution of a severe squall line over Oklahoma. *Mon. Wea. Rev.,* **113,** 1563–1589.

Holland, G. J., 1986: Interannual variability of the Australian summer monsoon at Darwin: 1952–82. *Mon. Wea. Rev.,* **114,** 594–604.

Houze, R. A., Jr., 1977: Structure and dynamics of a tropical squall-line system. *Mon. Wea. Rev.,* **105,** 1540–1567.

——, 1982: Cloud clusters and large-scale vertical motions in the tropics. *J. Meteor. Soc. Japan,* **60,** 396–410.

——, 1989: Observed structure of mesoscale convective systems and implications for large-scale heating. *Quart. J. Roy. Meteor. Soc.,* **115,** 425–461.

——, and E. N. Rappaport, 1984: Air motions and precipitation structure of an early summer squall line over the eastern tropical Atlantic. *J. Atmos. Sci.,* **41,** 553–574.

Johnson, R. H., 1982: Vertical motion of near-equatorial winter monsoon convection. *J. Meteor. Soc. Japan,* **60,** 682–690.

——, 1984: Partitioning tropical heat and moisture budgets into cumulus and mesoscale components: Implications for cumulus parameterization. *Mon. Wea. Rev.,* **112,** 1590–1601.

——, 1992: Heat and moisture sources and sinks of Asian monsoon precipitating systems. *J. Meteor. Soc. Japan,* **70,** 353–372.

——, and G. S. Young, 1983: Heat and moisture budgets of tropical mesoscale anvil clouds. *J. Atmos. Sci.,* **40,** 2138–2147.

——, W. A. Gallus, Jr., and M. D. Vescio, 1990: Near-tropopause vertical motion within the trailing stratiform region of a midlatitude squall line. *J. Atmos. Sci.,* **47,** 2200–2210.

Jorgensen, D. P., and M. A. LeMone, 1989: Vertical velocity characteristics of oceanic convection. *J. Atmos. Sci.,* **46,** 621–640.

Keenan, T. D., and R. E. Carbone, 1992: A preliminary morphology of precipitation systems in tropical northern Australia. *Quart. J. Roy. Meteor. Soc.,* **118,** 283–326.

——, and S. A. Rutledge, 1993: Mesoscale characteristics of monsoonal convection and associated stratiform precipitation. *Mon. Wea. Rev.,* **121,** 352–374.

Larsen, M. F., S. Fukao, O. Aruga, M. D. Yamanaka, T. Tsuda, and S. Kato, 1991: A comparison of VHF radar vertical-velocity measurements by a direct vertical-beam method and by a VAD technique. *J. Atmos. Oceanic Technol.,* **8,** 766–776.

Leary, C. A., and R. A. Houze, Jr., 1979: The structure and evolution of convection in a tropical cloud cluster. *J. Atmos. Sci.,* **36,** 437–457.

LeMone, M. A., and E. J. Zipser, 1980: Cumulonimbus vertical velocity events in GATE. Part I: Diameter, intensity, and mass flux. *J. Atmos. Sci.,* **37,** 2444–2457.

——, G. M. Barnes, E. J. Szoke, and E. J. Zipser, 1984: The tilt of the leading edge of mesoscale tropical convective lines. *Mon. Wea. Rev.,* **112,** 510–519.

Mapes, B., and R. A. Houze, Jr., 1992: An integrated view of the 1987 Australian monsoon and its mesoscale convective systems. Part II: Vertical structure. *Quart. J. Roy. Meteor. Soc.,* **119,** 733–754.

Petersen, W., 1992: Cloud-to-ground lightning in tropical mesoscale convective systems. M.S. thesis, Dept. of Atmospheric Science, Colorado State University, 225 pp. [Atmos. Sci. Paper No. 503.]

Ramage, C. S., 1968: Role of a tropical "Maritime Continent" in the atmospheric circulation. *Mon. Wea. Rev.,* **96,** 365–370.

Rasmussen, E. N., and S. A. Rutledge, 1993: Evolution of quasi-two-dimensional squall lines. Part I: Kinematic and reflectivity structure. *J. Atmos. Sci.,* **50,** 2584–2606.

Riehl, H., and J. S. Malkus, 1958: On the heat balance in the equatorial trough zone. *Geophysica,* **6,** 503–538.

Rutledge, S. A., R. A. Houze Jr., M. I. Biggerstaff, and T. Matejka, 1988: The Oklahoma–Kansas mesoscale convective system of 10–11 June 1985: Precipitation structure and single–Doppler radar analysis. *Mon. Wea. Rev.,* **116,** 1409–1430.

——, E. R. Williams, and T. D. Keenan, 1992: The Down Under Doppler and Electricity Experiment (DUNDEE): Overview and preliminary results. *Bull. Amer. Meteor. Soc.,* **73,** 3–16.

Sato, T., H. Doji, H. Iwai, I. Kimura, S. Fukao, M. Yamamoto, T. Tsuda, and S. Kato, 1990: Computer processing for deriving drop-size distributions and vertical air velocities from VHF Doppler radar spectra. *Radio Sci.,* **25,** 961–973.

Simpson, J., R. F. Adler, and G. R. North, 1988: A proposed Tropical Rainfall Measuring Mission (TRMM) satellite. *Bull. Amer. Meteor. Soc.,* **69,** 278–295.

——, T. D. Keenan, B. Ferrier, R. H. Simpson, and G. J. Holland, 1993: Cumulus mergers in the Maritime Continent region. *Meteor. Atmos. Phys.,* **51,** 73–99.

Smull, B. F., and R. A. Houze, Jr., 1987: Dual-Doppler radar analysis of a midlatitude squall line with a trailing region of stratiform rain. *J. Atmos. Sci.,* **44,** 2128–2148.

Szoke, E. J., E. J. Zipser, and D. P. Jorgensen, 1986: A radar study of convective cells in mesoscale systems in GATE. Part I: Vertical profile statistics and comparison with hurricanes. *J. Atmos. Sci.,* **43,** 182–197.

Wakasugi, K., A. Mizutani, M. Matsuo, S. Fukao, and S. Kato, 1986: A direct method for deriving drop-size distribution and vertical air velocities from VHF Doppler radar spectra. *J. Atmos. Oceanic Technol.,* **3,** 623–629.

——, A. Mizutani, M. Matsuo, S. Fukao, and S. Kato, 1987: Further discussion on deriving drop-size distribution and vertical air velocities directly from VHF Doppler radar spectra. *J. Atmos. Oceanic Technol.,* **4,** 170–179.

Webster, P. J., and R. A. Houze Jr., 1991: The Equatorial Mesoscale Experiment (EMEX): An overview. *Bull. Amer. Meteor. Soc.,* **72,** 1481–1503.

Williams, E., and W. Ecklund, 1992: 50 MHz profiler observations of trailing stratiform precipitation: Constraints on microphysics and in situ charge separation. Preprints, *11th Int. Conf. on Clouds and Precipitation,* Montreal, Canada, ICCP, Int. Assoc. of Meteor. Atmos. Phys., 754–757.

Yoe, J. G., M. F. Larsen, and E. J. Zipser, 1992: VHF wind-profiler data quality and comparison of methods for deducing horizontal and vertical air motions in a mesoscale convective storm. *J. Atmos. Oceanic Technol.,* **9,** 713–727.

Zipser, E. J., and M. A. LeMone, 1980: Cumulonimbus vertical velocity events in GATE. Part II: Synthesis and model core structure. *J. Atmos. Sci.,* **37,** 2458–2469.